Ore Geology Reviews 139 (2021) 104574

Contents lists available at ScienceDirect

Ore Geology Reviews

journal homepage: www.elsevier.com/locate/oregeorev

In situ trace elements of magnetite in the Bayan Obo REE-Nb-Fe deposit: Implications for the genesis of mesoproterozoic iron mineralization

Hai-Dong She [a,b], Hong-Rui Fan [a,b,c,d,*], Kui-Feng Yang [a,b,c,d], Xiao-Chun Li [a,b,c], Qi-Wei Wang [d], Li-Feng Zhang [d], Shang Liu [e], Xing-Hui Li [a,c], Zhi-Hui Dai [f]

[a] Key Laboratory of Mineral Resources, Institute of Geology and Geophysics, Chinese Academy of Sciences, Beijing 100029, China
[b] College of Earth and Planetary Sciences, University of Chinese Academy of Sciences, Beijing 100049, China
[c] Innovation Academy for Earth Science, Chinese Academy of Sciences, Beijing 1000029, China
[d] State Key Laboratory of Baiyunobo Rare Earth Resource Researches and Comprehensive Utilization, Baotou Research Institute of Rare Earths, Baotou 014030, China
[e] School of Earth Sciences and Key Laboratory of Mineral Resources in Western, China (Gansu Province), Lanzhou University, Lanzhou 730000, China
[f] State Key Laboratory of Deposit Geochemistry, Institute of Geochemistry, Chinese Academy of Sciences, Guiyang 550081, China

ARTICLE INFO

Keywords:
Trace elements
LA-ICP-MS
Magnetite
Bayan Obo deposit
China

ABSTRACT

The giant Bayan Obo REE deposit bears a large amount of iron resources as well. However, the genesis of iron mineralization is still highly controversial with limited research. In this study, new data of trace elements of magnetite from Bayan Obo ores, Eastern contact zone skarn and Heinaobao BIF are obtained by Laser ablation (LA) ICP-MS analyses, revealing the genesis of Bayan Obo iron resources through comparing study. The Bayan Obo deposit contains disseminated, banded and massive ores, and in which magnetite is associated with REE minerals, fluorite, aegirine, riebeckite, and biotite. Euhedral magnetite in the skarn of Eastern contact zone is usually associated with pyrite, biotite, fluorite, and bastnaesite. There are two types of magnetite in the Heinaobao BIF: (1) euhedral to subhedral magnetite associated with quartz and a small amount of amphibole; (2) anhedral magnetite associated with quartz, garnet, plagioclase, amphibole and biotite.

Magnetite in the Bayan Obo is enriched in Ni, but depleted in Mg, Al, Ti, Ge, Mn, Ga and Zn, showing low and variable concentrations, which is similar to the hydrothermal magnetite. The contents of some trace elements (e.g. Ti, Mn, Sc, Zn, Nb and REE) of magnetite from the skarn ores are generally higher, indicating a relatively high formation temperature. Magnetite in the Heinaobao BIF is generally characterized by low and uniform trace element contents, except for the abnormal values of Ti, Al, Cr and Mn, suggesting the involvement of terrigenous clastic materials. Compared with Bayan Obo magnetite, the skarn magnetite has the highest Sn/Ga, Co/Ni, Nb/Ta, La/Yb, Ti/V and Ti/Al ratios, while magnetite in the BIF has the highest Al/Co and lowest Nb/Ta ratios. The significant difference in mineralogical and trace element characteristics among the three types of magnetite indicates that the iron resources in Bayan Obo deposit are unlikely to be a skarn Fe deposit nor a BIF deposit. However, the Bayan Obo magnetite shows similar geochemical characteristics to hydrothermal magnetite related to carbonatite, both of which are depleted in high field strength elements, such as Zr, Hf and Ta, and show strong positive anomalies of Mn and Zn and negative anomalies of Co and Ga. In addition, in the diagrams of Ti vs. Nb + Ta and Ti vs. Zr + Hf, the Bayan Obo magnetite falls into the field of hydrothermal magnetite associated with carbonatite. In conclusion, it is recommended that the Bayan Obo iron deposit is a typical hydrothermal deposit related to carbonatite. In this contribution, the skarn magnetite formed at high temperature and the BIF magnetite was contaminated by terrigenous materials deviating from the expected region in discriminant diagrams. It is therefore proposed that the validity of these diagrams depends on a full understanding of mineralogical characteristics of samples and magnetite precipitation environment, and that multiple discrimination diagrams should be used in combination.

* Corresponding author at: Key Laboratory of Mineral Resources, Institute of Geology and Geophysics, Chinese Academy of Sciences, Beijing 100029, China.
E-mail address: fanhr@mail.iggcas.ac.cn (H.-R. Fan).

https://doi.org/10.1016/j.oregeorev.2021.104574
Received 31 August 2021; Received in revised form 3 November 2021; Accepted 6 November 2021
Available online 11 November 2021

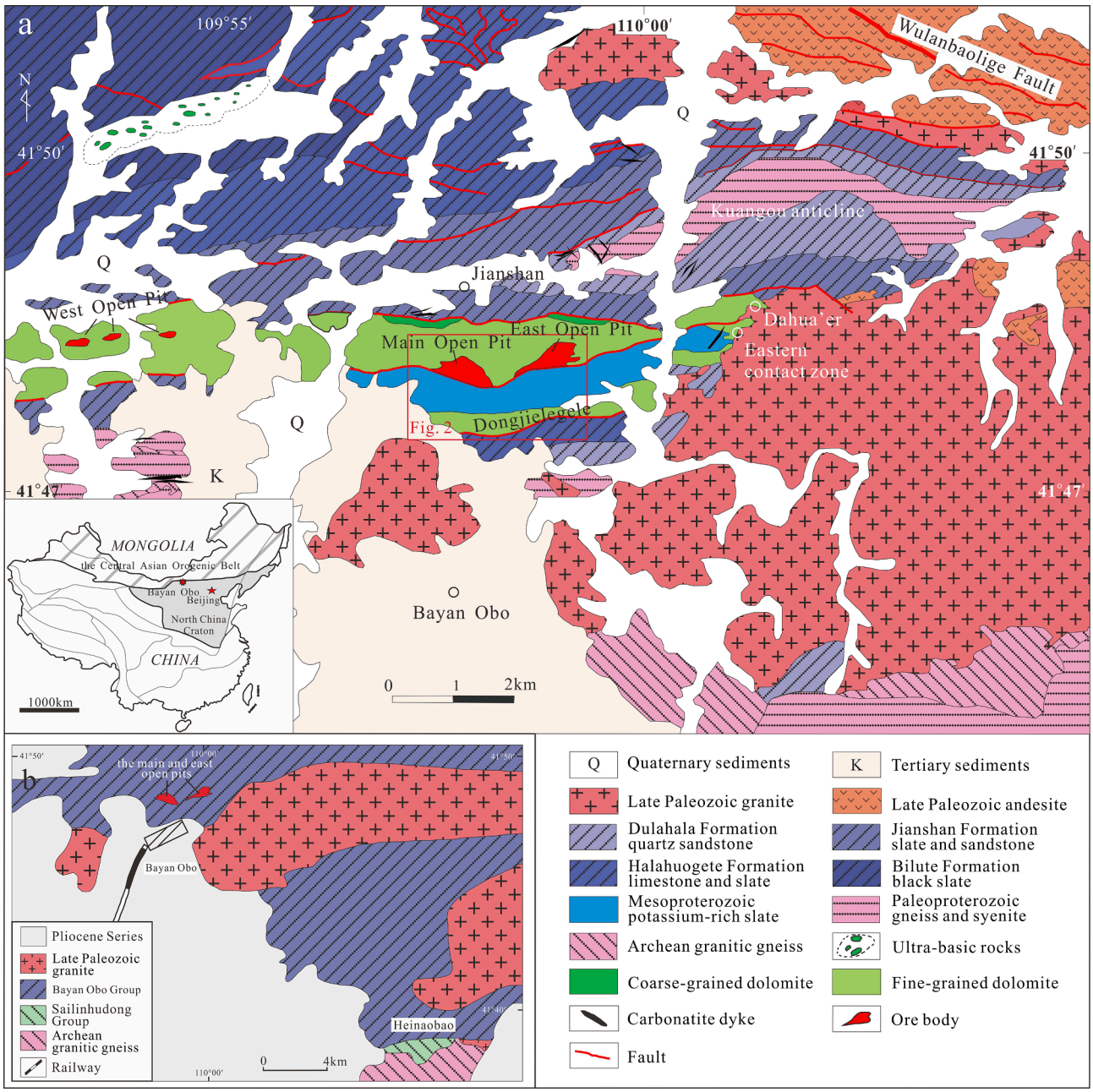

Fig. 1. a: Geographic location and Geological sketch map [revised from Yang et al. (2011)] of the Bayan Obo REE-Nb-Fe deposit. b: regional geological schematic map of Bayan Obo-Heinaobao area (revised from unpublished geological record).

1. Introduction

The giant and unique Bayan Obo REE-Nb-Fe deposit, the world's main supplier of light rare earth resources, has been widely concerned by academia and industry (references in Smith et al., 2015; Fan et al., 2016; Yang et al., 2017). Since the discovery of the giant REE deposit by Mr. Zuolin He in 1935, a large number of studies on rare earth mineralogy, mineralization chronology, geochemistry of carbonatite and sources of ore-forming fluids have been carried out in previous works (Campbell and Henderson, 1997; Le Bas et al., 2007; Shimazaki et al., 2008; Yang et al., 2011; Smith and Spratt, 2012; Ribeiro Da Costa et al., 2013; Campbell et al., 2014; Ling et al., 2014; Lai et al., 2016; Zhang et al., 2017; Song et al., 2018; Yang et al., 2019; Chen et al., 2020; Li et al., 2021; She et al., 2021). In contrast, limited attention has been paid to the genesis of iron mineralization, considering the fact that it is also a large iron ore deposit with iron reserves of more than 1500 million tonnes (iron oxide average grade 35%; Drew et al., 1990; Chao et al., 1997; Hao et al., 2002), and Bayan Obo's three large open pits were primarily designed according to the distribution of iron ore bodies (Fig. 1a). Based on the banded structures in typical ore, and oxygen isotope as well as *in-situ* trace element data sets of magnetite, some scholars suggested that the Bayan Obo Fe resources were initially enriched in a Mesoproterozoic sedimentary deposit, simultaneously with the formation of the Bayan Obo Group in a rift basin, and the Fe resources were later modified and re-enriched by hydrothermal fluids (Wei and Shangguan, 1983; Zeng et al., 1981; Institute of Geochemistry, Chinese Academy of Sciences, 1988; Cao et al., 1994; Huang et al., 2015; Yang et al., 2015, 2017). However, other researchers found that the iron isotope of geological units indicates a magmatic origin (δ^{56}Fe: 0‰), combining with geochemistry of the minerals associated with magnetite, and proposed that this deposit is a differentiation product of magmatic-hydrothermal system related to carbonatite (Zhou et al., 1980; Bai et al.,

1996; Zhang et al., 2003; Sun et al., 2011, 2012, 2013).

Magnetite ($Fe^{3+}[Fe^{2+}Fe^{3+}]O_4$) is one of the most abundant oxide minerals of the spinel group in the earth's crust. It is also a common accessory mineral in igneous rocks, metamorphic rocks and sedimentary rocks, and distributes in various types of deposits as major or minor component (Righter et al., 2006; Nadoll et al., 2014; Milani et al., 2017; Verdugo-Ihl et al., 2020; Ebotehouna et al., 2021; Peng et al., 2021; Tian et al., 2021). In different metallogenic environments, controlled by different physical and chemical conditions (such as source rock composition, temperature, oxygen fugacity, sulfur fugacity, pressure, coexisting minerals and cooling rate; Whalen and Chappel, 1988; Frost and Lindsley, 1991; Ghiorso and Sack, 1991; Ryabchikov and Kogarko, 2006; Rusk et al., 2009; Dupuis and Beaudoin, 2011; Dare et al., 2012; Mollo et al. 2013; Nadoll et al., 2015; Huang et al., 2019a,b; Duran et al., 2020), magnetite would contain different amounts and combinations of trace elements (e.g. Mg, Al, Sc, Ti, V, Cr, Mn, Co, Ni, Zn, Ga, Ge, Y, Nb, Ta and Zr) in its spinel structure during the formation processes (Carew et al., 2006; Rusk et al., 2009; Dupuis and Beaudoin, 2011; Nadoll et al., 2014, 2015; Knipping et al., 2015). These variations in compositions make magnetite a useful petrogenetic indicator and pathfinder mineral, for fingerprinting mineralization types and reconstructing detailed mineralization processes (Barnes and Roeder, 2001; Carew et al., 2006; Reguir et al., 2008; Beaudoin and Dupuis, 2009; Dupuis and Beaudoin, 2011; Nadoll et al., 2012; Dare et al., 2012, 2014; Palma et al., 2020; Ebotehouna et al., 2021). In the past few decades, a large number of geochemical studies have revealed that the differences in trace elements of magnetite crystallized in the magmatic, the hydrothermal, the sedimentary, the mineralized and the non-mineralized environments. For example, concentrations of elements such as Al, Ti, V, Cr, Ni, and Ga in igneous magnetite were significantly higher than that of hydrothermal magnetite, while hydrothermal-metamorphic magnetite from BIF is at the lower end of the temperature spectrum and has the lowest overall concentration of trace elements among all types of magnetite (Ray and Webster, 2007; Beaudoin and Dupuis, 2009; Rusk et al., 2009; Dupuis and Beaudoin, 2011; Nadoll et al., 2012, 2014, 2015; Knipping et al., 2015). Magnetite from mafic and ultramafic igneous rocks tends to have a higher concentration of Ti than that crystallized from felsic to intermediate magmas (e.g., Grigsby, 1990; Lindsley, 1991; Dare et al., 2012). Rusk et al. (2010) pointed out that the Ti/Mn ratio of hydrothermal magnetite is an effective discriminative index between barren and mineralization systems, and among different deposits. A series of statistical analyses of the compositional variation between igneous and hydrothermal magnetites have led to numerous discriminant diagrams and indicators, such as the plots of Ni + Cr vs. Si + Mg, Al/(Zn + Ga) vs. Cu/(Si + Ca), Ni/(Cr + Mn) vs. Ti + V, Ca + Al + Mn vs. Ti + V, Ti vs. Ni/Cr, and the indicative ratios of Sn/Ga, Ti/V, Ti/Mn and Al/Co (Singoyi et al., 2006; Kamvong et al., 2007; Rusk et al., 2010; Dupuis and Beaudoin, 2011; Dare et al., 2014; Nadoll et al., 2014; Knipping et al., 2015; Duran et al., 2020; Aftabi et al., 2021).

Magnetite, one of the most important ore minerals in the Bayan Obo deposit, is a direct medium to study the genesis of large-scale iron mineralization. In this contribution, we collected disseminated, banded and massive ores from the Main and the East open pits of the Bayan Obo deposit, skarn ores from the Eastern contact zone and banded iron formation (BIF) from the nearby Heinaobao iron deposit. Based on observation of different types of ores under reflected polarizing microscope and scanning electron microscope, *in-situ* trace element analysis of various magnetites was carried out by laser ablation inductively coupled plasma mass spectrometry (LA-ICP-MS). The data make it possible to compare chemical compositions of different types of magnetite from the Bayan Obo, Eastern contact zone and Heinaobao, and also provide strong evidences of the origin of the large-scale iron mineralization in Bayan Obo deposit.

2. Geological setting

2.1. Archean-Mesoproterozoic sequences

The Bayan Obo REE deposit is located at the northern margin of the North China Craton, adjacent to the Central Asian Orogenic Belt in the north (Fig. 1a). The first fault in the area is the Wulanbaolige deep fault, also known as the Bayan Obo-Chifeng fault, located about 10 km to the north of Bayan Obo deposit. The secondary fault is the Baiyinjiaolake-Bayan Obo fault. The eastern part of this fault is also known as the Kuangou fault, which is roughly east–west trending and cut off by Wulanbaolige fault. There is a set of Archean-Paleoproterozoic metamorphic basement complexes, including the Archean granite-gneiss distributed in the southeast of the mining area, the Early Proterozoic granodiorite, syenite and biotite gneiss in the core of Kuangou anticline and the south of the Main open pit, and the late Early Proterozoic garnet-bearing gneiss in the south of the East open pit (Fan et al., 2010).

The Bayan Obo Group, a set of Paleoproterozoic-Mesoproterozoic rift sedimentary formations (Fig. 1a), is a suite of extremely thick weak-metamorphic sedimentary rock sequences, un-conformably covering the metamorphic basement rock series in the area, with a total thickness of nearly 10 km. The main rock types are clastic rocks, shale and carbonate rocks. In the Bayan Obo area, this set of strata is widely distributed in the two limbs of the Kuangou anticline. There are obvious differences between the strata on the north and south sides of the Kuangou fault: the strata on the south side have undergone intense thermal transformation with high degree of metamorphism, while the thermal event has little influence on the north side (Institute of Geochemistry, Chinese Academy of Sciences, 1988). According to the lithological characteristics, the Bayan Obo Group can be divided into six rock formations (Dulahala Formation, Jianshan Formation, Halahuogete Formation, Bilute Formation, Baiyinbaolage Formation and Hujiertu Formation) and eighteen rock sections. It is generally believed that the Bayan Obo Group was formed during the Paleoproterozoic to the Mesoproterozoic (Yang et al., 2012; Zhong et al., 2015; Lai et al., 2016; Zhou et al., 2018).

More than 100 carbonatite dykes expose around the open pits, which intruded into the Bayan Obo Group in the Mesoproterozoic (Zhang et al., 2003; Fan et al., 2006; Yang et al., 2011; Liu et al., 2018b), and metamorphic basement complexes. According to their mineral compositions, they can be divided into three types: the dolomite-, the dolomite-calcite- and the calcite- types (Fan et al., 2006).

2.2. Paleozoic sequences

Paleozoic granitoids (including granodiorite, monzogranite, and biotite granite) are widely distributed in the southeast of the East open pit and the south of the West open pit (Fig. 1a). These granitoids were formed between 263 Ma and 281 Ma (peaking at 269 Ma; Fan et al., 2009), in a geodynamic setting related to the continent–continent collision in the late stage of Paleo-Asian Ocean closure (Wang et al., 1994; Chao et al., 1997; Xiao et al., 2003; Fan et al., 2009). There also exist slightly earlier gabbro intrusions (Bai et al., 1996; Institute of Geochemistry, Chinese Academy of Sciences, 1988). Most of them intruded into the stratum as rock stocks or dikes, which are cut through by granite bodies or developed as xenoliths inside granite bodies.

2.3. Bayan Obo and other types of Fe deposits in the area

The Bayan Obo area contains the vast majority of rare earth resources in the world, especially light rare earth elements, while the region also has a large number of iron resources with various types. According to metallogenic types, iron resources in Bayan Obo region are mainly classified into three categories: (1) iron orebodies associated with rare earth resources in the Bayan Obo deposit, (2) BIF-type iron deposit in Heinaobao (Fig. 1b), 3 skarn iron deposit on the Eastern

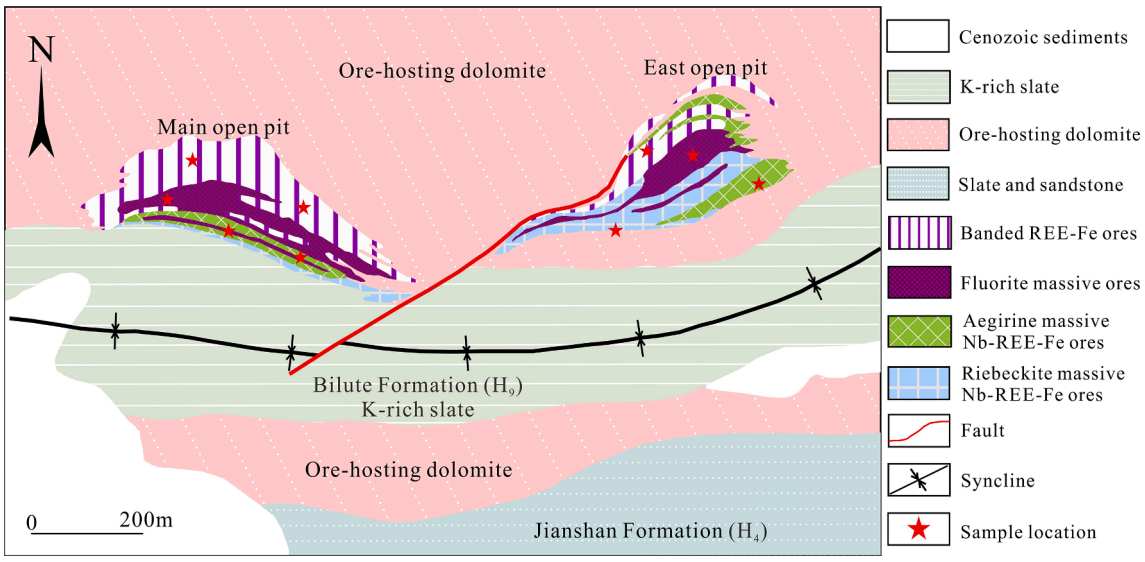

Fig. 2. Geological sketch and mineralization zoning map of Main and East open pits at Bayan Obo. Modified from Institute of Geochemistry, Chinese Academy of Sciences (1988) and Liu et al. (2018a).

contact zone (Fig. 1a).

Bayan Obo: Iron orebodies are located near the intersection of Wulanbaolige fault and Kuangou fault. The deposit is comprised of East open pit, Main open pit and West open pit gradually merged by dozens of small mines (Fig. 1a). The lenticular ore bodies strike nearly E-W and incline southward, and are hosted in a set of nearly EW-trending dolomites, which are further divided into north and south parts by the slate of the Bilute formation. The alkaline metasomatism of the Main and East open pits is very strong, mainly consisting of a set of alkaline mineral assemblage represented by aegirine and riebeckite. Based on mineral assemblage, the Fe ores in the Bayan Obo REE-Nb-Fe deposit are generally classified into dolomite-dominating REE-Nb-Fe ore, banded REE-Nb-Fe ore, massive fluorite-rich Fe ore, massive aegirine-rich REE-Nb-Fe ore and massive Na-amphibole-rich REE-Nb-Fe ore (Fig. 2; Institute of Geochemistry, Chinese Academy of Sciences, 1988). The main rare earth minerals in the mining area are monazite, bastnaesite, parisite, cebaite, huanghoite, etc. The Niobium-bearing minerals are mainly fergusonite-(Y), columbite, aeschynite, pyrochlore and baotite, and the iron ore minerals are magnetite and hematite (Chao et al., 1991; Fan et al., 2016).

Heinaobao: Heinaobao BIF type iron deposit is located 25 km southeast of Bayan Obo (Fig. 1b). The iron ore bodies occur in the amphibole-plagioclase gneiss of the Wulashan Group in the Neoarchean in the form of stratiform or stratoid. The ore minerals are mainly magnetite, and a small amount of hematite and limonite can be seen locally. The gangue minerals are quartz, plagioclase, and a small amount of biotite and amphibole. The iron ore is often in medium-fine grained crystalloblastic texture and dense block structure with iron oxide average grade of 31 wt% (referring to mine exploration data). Previous studies have shown that the BIF type deposits in this area were mixed with terrigenous clastic materials to varying degrees during the formation (Nan et al., 2017), and experienced metamorphism of greenschist to low-amphibolite facies with the highest temperature of 500–650 °C after the formation of BIF (Liu, 1996; Zhang et al., 2012; Liu et al., 2014). These factors result in the existence of two types of ores in the Heinaobao BIF deposit. One is mainly composed of quartz and magnetite with a trace amount of amphibole, and the other is mainly composed of magnetite, quartz, plagioclase, garnet, amphibole and biotite. On the whole, the morphology of ore-bodies, country rock characteristics, ore texture and mineral composition of the Heinaobao deposit are extremely similar to those of the BIF type iron deposit in the adjacent Baotou-Guyang area (Shen, 2012; Zhang et al., 2012; Liu et al., 2014; Wang et al., 2019).

Eastern Contact Zone (ECZ): skarn is widely distributed in the Eastern contact zone about 3 km to the east of the East open pit (Fig. 1a), which is the product of the metasomatism between the Hercynian granitic intrusions and the ore-hosting dolomite. The main skarn minerals include diopside, tremolite, humite, phlogopite, fluorite, magnetite and pyrite (Fan et al., 2002). The iron orebodies are distributed in beaded shape with small scale.

3. Sampling and petrography

The samples used in this study include the following: 1) the disseminated, the banded and the massive ores distributed in the Main and East open pits of the Bayan Obo deposit; 2) skarns in the Eastern contact zone; 3) BIF type iron ores in Heinaobao. All types of magnetite particles prepared for LA-ICP-MS spot analysis were petrographically observed by reflective light microscope and scanning electron microscope in detail to avoid possible contamination from mineral inclusions. The diameter of hematite from Bayan Obo was smaller than that of the laser beam spot and was not used in this study.

The disseminated ores constitute the main part of ore-hosting dolomite in Bayan Obo (Fig. 2). The main minerals are dolomite, calcite, monazite, bastnäsite, fluorite and magnetite (Fig. 3a), as well as a small amount of fersmite, ilmenorutile and fergusonite. Magnetite particles are disseminated in the form of granular or granular aggregate between fine-grained dolomite particles (Fig. 4a), euhedral to subhedral, and their distribution is extremely uneven. The associated mineral assemblages of magnetite include fluorite, monazite, bastnäsite and apatite, and there are a large number of mineral inclusions of monazite, apatite and dolomite at the central of magnetite particles (Fig. 4b).

The banded ore is mainly distributed on the north side of the Main and East open pits (Fig. 2). The aggregate of magnetite, bastnäsite, monazite, aegirine and fluorite are often banded in this type of Fe ores (Fig. 3b). The magnetite particles are subhedral to anhedral with a small diameter of less than 100 μm, and are usually associated with fluorite, apatite, aegirine, rare earth minerals, and baryte (Fig. 4c). They are usually interbedded with rare earth minerals, fluorite and aegirine in the form of granular aggregates, and the magnetite particles are strongly dynamic modified after formation (Fig. 4d).

The massive ores are mainly distributed in the middle of the Main and East open pits (Fig. 2). The ore has a dense block structure and its mineral composition includes fluorite, magnetite, aegirine, riebeckite,

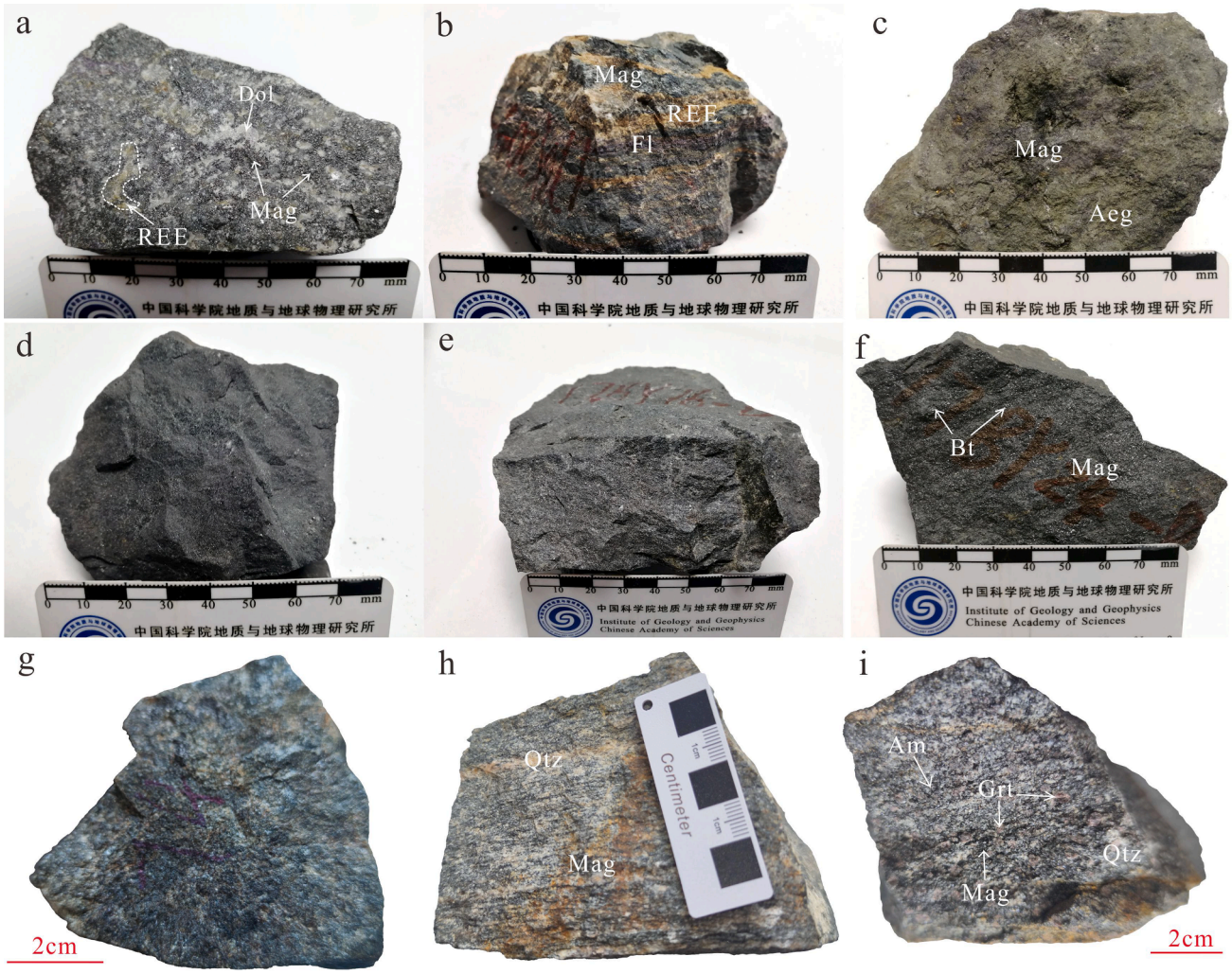

Fig. 3. Photographs of hand specimens of different types of ores from the East and Main open pits of Bayan Obo, Eastern contact zone and Heinaobao. a: disseminated ore; b: banded ore with bands of magnetite, fluorite and rare earth minerals; c: aegirine-type massive ore; d: fluorite-type massive ore; e: sodic amphibole-type massive ore; f: biotite-type massive ore; g: skarn-type iron ore in the Eastern contact zone; h: banded iron formation with bands of magnetite and quartz in Heinaobao; i: banded iron formation with the assemblages of garnet, magnetite, quartz and amphibole in Heinaobao. Aeg: aegirine; Am: amphibole; Bt: biotite; Dol: dolomite; Fl: fluorite; Grt: garnet; Mag: magnetite; Qtz: quartz; REE: rare earth minerals.

biotite, bastnäsite, huanghoite, monazite and apatite. According to the main mineral composition, it can be divided into fluorite-, aegirine-, mica-, and riebeckite-type massive ores (Fig. 3c-f). The magnetite particles have euhedral to subhedral shape, and are usually distributed among hydrothermal minerals (e.g. fluorite, aegirine, riebeckite and biotite) in the form of granular or granular aggregates (Fig. 4e-l). The associated mineral assemblages of magnetite include aegirine, fluorite, biotite, riebeckite, bastnäsite, monazite, apatite and a small amount of quartz, albite and parisite, and there also exist mineral inclusions of bastnäsite, riebeckite and siderite in magnetite (Fig. 4j).

The skarn orebody in the Eastern contact zone is small and the rich orebody has been mined, so the skarn samples used in this study are mainly collected from the endoskarn near the granitic pluton. This kind of ore is a dense massive structure with low grade of iron (Fig. 3g), and the main minerals include sodic-pyroxene, edenite, albite, phlogopite, pyrite and magnetite. Magnetite is distributed in the form of granular, usually associated with minerals such as pyrite, biotite, fluorite and bastnäsite (Fig. 4m).

The Heinaobao samples in this study include the following two types: 1) BIF with quartz and magnetite as the main minerals, banded structure (Fig. 3h). The magnetite particles are euhedral to subhedral, and coexist with quartz and a small amount of amphibole (Fig. 4n); 2) BIF contains abundant garnet, plagioclase and amphibole, with dense massive structure (Fig. 3i). Magnetite grains have subhedral to anhedral shape and are usually closely associated with quartz, garnet, amphibole, plagioclase and biotite (Fig. 4o-p). For the sake of the following description, we name the above two kinds of BIF as normal BIF (N-BIF) and garnet-bearing BIF (G-BIF) respectively.

4. Analytical methods

Trace elements analyses of magnetite were conducted by an Agilent 7700x quadrupole ICP-MS coupled to an ASI RESOLution-LR-S155 laser microprobe equipped with a Coherent Compex-Pro 193 nm ArF excimer laser at the State Key Laboratory of Ore Deposit Geochemistry, Institute of Geochemistry, Chinese Academy of Sciences (IGCAS). Helium was applied as a carrier gas which was mixed with Argon via a T-connector before entering the ICP-MS. Each analysis consists of approximately 30 s of background acquisition (gas blank), followed by 50 s of data collection from the sample. The analysis was carried out under the condition of 40 μm pit size and 4 Hz pulse frequency. Detailed operating conditions for the laser ablation system and the ICP-MS instrument and data reduction are similar as described by Liu et al. (2008). A total of 42 elements were analyzed using isotopes ^{25}Mg, ^{27}Al, ^{29}Si, ^{42}Ca, ^{45}Sc, ^{49}Ti,

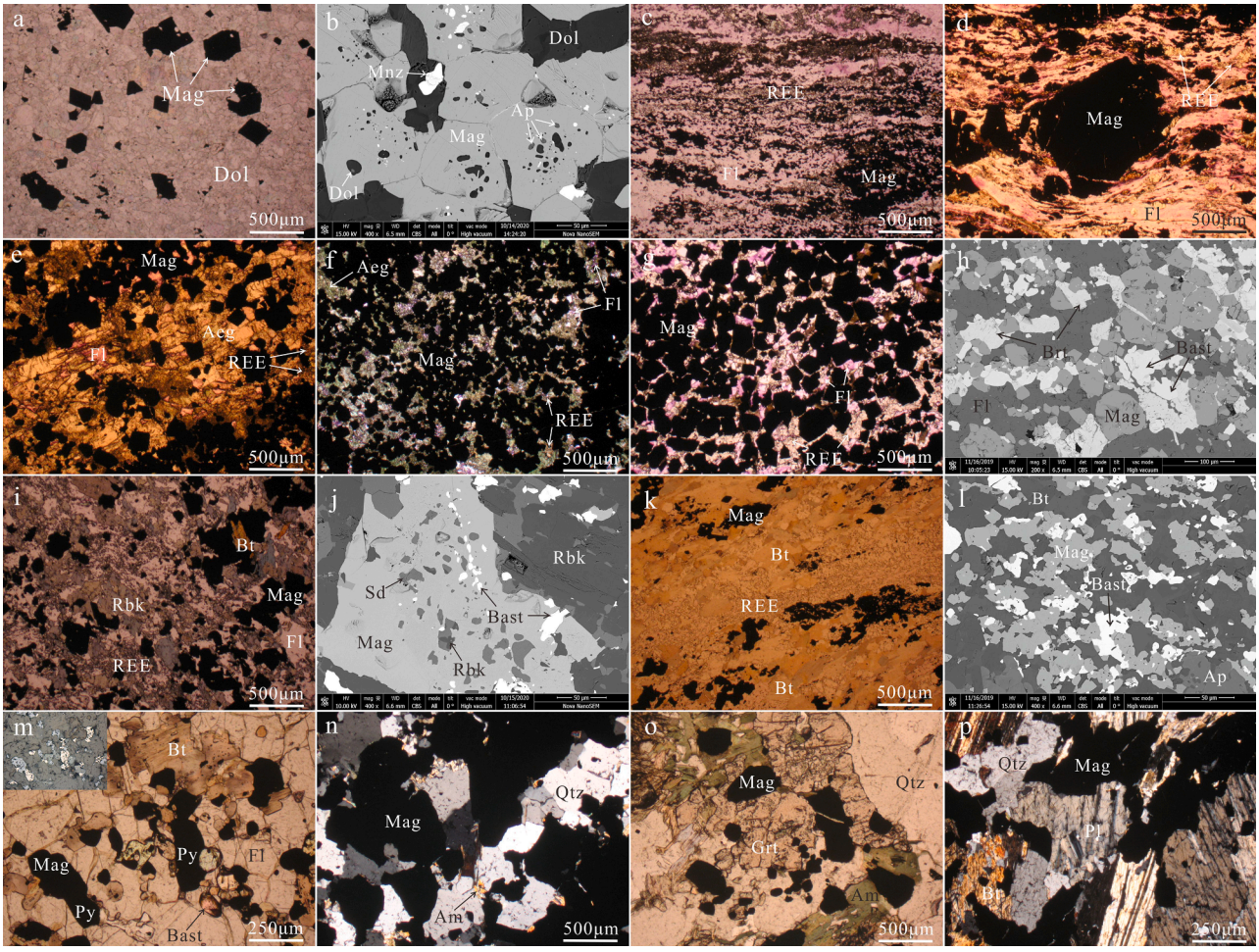

Fig. 4. Magnetite morphology and mineral association in different types of ores. a: euhedral- subhedral magnetite in disseminated ore; b: the mineral inclusions of apatite, monazite and dolomite at the center of magnetite grains in disseminated ore; c: the band of magnetite aggregates in banded ore; d: magnetite particles subjected to strongly dynamic modification in banded ore; e-f: subhedral magnetite associated with aegirine, rare earth minerals and fluorite in aegirine-type massive ore; g-h: euhedral to subhedral magnetite associated with fluorite, baryte and bastnäsite in fluorite-type massive ore; i: anhedral magnetite associated with riebeckite, rare earth minerals and a small amount of biotite in sodic amphibole-type massive ore; j: the mineral inclusions of bastnäsite, riebeckite and siderite in anhedral magnetite of sodic amphibole-type massive ore; k-l: anhedral magnetite aggregates associated with biotite, bastnäsite and apatite in biotite-type massive ore; m: the associated mineral assemblages of magnetite include biotite, pyrite, fluorite and bastnäsite in the Eastern contact zone skarn (the upper left corner is the reflected polarizing light photograph at the same position); n: euhedral-subhedral magnetite associated with quartz and a small amount of amphibole in banded iron formation of Heinaobao N-BIF; o-p: subhedral magnetite associated with garnet, quartz, amphibole, biotite and plagioclase of Heinaobao G-BIF. Aeg: aegirine; Am: amphibole; Ap: apatite; Bast: bastnäsite; Bt: biotite; Brt: baryte; Dol: dolomite; Fl: fluorite; Grt: garnet; Mag: magnetite; Mnz: monazite; Pl: plagioclase; Py: pyrite; Qtz: quartz; REE: rare earth minerals; Rbk: riebeckite: Sd: siderite.

^{51}V, ^{53}Cr, ^{55}Mn, ^{59}Co, ^{60}Ni, ^{65}Cu, ^{66}Zn, ^{71}Ga, ^{74}Ge, ^{88}Sr, ^{89}Y, ^{90}Zr, ^{93}Nb, ^{95}Mo, ^{118}Sn, ^{137}Ba, ^{139}La, ^{140}Ce, ^{141}Pr, ^{143}Nd, ^{147}Sm, ^{151}Eu, ^{155}Gd, ^{159}Tb, ^{163}Dy, ^{165}Ho, ^{166}Er, ^{169}Tm, ^{173}Yb, ^{175}Lu, ^{178}Hf, ^{181}Ta, ^{209}Bi, $^{Total}Pb$, ^{232}Th and ^{238}U. Element contents were calibrated against multiple-reference materials (GSE-1G, BCR-2G, BIR-1G, GOR-128 and BHVO-2G) using ^{57}Fe as the internal standardization (Gao et al., 2013). The preferred element concentration values for the USGS reference glasses are from the GeoReM database (http://georem.mpch-mainz.gwdg.de/). Every ten analyses of samples were followed by one analysis of GSE-1G and BC-28 as quality control to correct the time-dependent drift of sensitivity and mass discrimination. Off-line selection and integration of background and analyte signals, and time-drift correction and quantitative calibration were performed by ICPMSDataCal (Liu et al., 2008).

The major elements analyses of magnetite were performed on a JEOL JXA-8230 electron microprobe (EMPA) at the Wuhan Sample Solution Analytical Technology Co., Ltd, Hubei, China, which was operated with a 15 kV accelerating voltage and a 20 nA beam current with a 1 μm spot diameter. The peak counting time was 10 s for Ti, Sn, Al, Fe, Mn, Zn, Mg, Ga, V and Co, and 20 s for Ca and Si. The background counting times were half of the peak counting time at both high and low energy background positions. Calibration standards used were magnetite for Fe, olivine for Mg, pyrope for Al, quartz for Si, johannsenite for Ca, rutile for Ti, cassiterite for Sn, and alloy or pure metal for Mn, Zn, Ga, V and Co. The detection limits for each element were Ca (150 ppm), Ti (270 ppm), Sn (380 ppm), Si (160 ppm), Al (150 ppm), Fe (258 ppm), Mn (188 ppm), Co (233 ppm), Mg (110 ppm), Ga (200 ppm), Zn (424 ppm), and V (200 ppm). ZAF calibration procedures were used for data correction. Iron concentrations determined by electron microprobe analyses were used as an internal standard for calibration of LA-ICP-MS data.

5. Analytical results

The major and trace element contents of various magnetites were determined by EMPA and LA-ICP-MS, respectively. A total of 42 elements, including 14 rare earth elements, were analyzed for magnetite, and most samples contain Cu, Th, and U below the detection limits, and therefore are unlikely to be used to investigate the geochemistry of

Table 1
The statistical result of LA-ICP-MS on magnetites in the Bayan Obo deposit, Eastern contact zone and Heinaobao.

	Item	Mg	Al	Si	Ca	Sc	Ti	V	Cr	Mn	Co	Ni	Zn	Ga	Ge	Sr	Y	Zr	Nb	Mo	Sn
Disseminated ore	Average	89.493	66.890	781.475	787.804	10.009	330.492	######	5.660	621.558	21.329	#####	118.263	2.204	2.117	7.402	2.005	0.037	7.064	1.952	5.505
	Median	84.434	76.217	569.525	55.676	6.393	313.698	######	1.741	625.259	21.359	#####	110.884	2.202	2.126	0.188	0.320	0.014	0.927	0.064	4.861
	Std Dev	25.394	34.726	523.981	#######	8.711	150.770	11.948	7.652	295.217	1.234	#####	35.075	0.516	0.234	#####	5.544	0.051	12.112	8.062	2.635
	Maximum	133.589	168.069	#######	#######	35.546	797.069	######	31.095	#######	23.738	#####	187.565	3.074	2.534	#####	25.169	0.178	38.116	37.092	12.479
	Minimum	53.543	20.784	403.734	bdl	2.994	161.437	######	0.000	294.776	18.995	#####	76.969	1.318	1.512	0.007	0.000	0.000	0.074	bdl	1.864
Banded ore	Average	89.151	32.980	537.687	86.024	4.686	225.498	64.160	0.668	#######	11.297	#####	117.462	1.602	1.426	0.431	1.953	0.336	8.732	1.349	6.240
	Median	90.682	38.444	503.339	43.661	2.596	180.782	56.391	0.418	#######	10.046	#####	84.508	1.486	1.167	0.160	0.177	0.025	1.928	0.012	5.624
	Std Dev	51.857	17.455	88.273	137.799	4.684	118.575	24.513	0.685	380.116	3.749	#####	69.255	0.506	0.632	0.657	5.597	0.913	19.620	5.547	1.960
	Maximum	195.359	56.416	818.725	565.659	19.069	435.933	######	2.168	#######	17.989	#####	347.424	2.450	2.474	2.467	26.079	4.064	89.552	26.006	11.358
	Minimum	22.168	7.068	419.045	bdl	0.625	102.295	38.140	0.000	728.921	7.242	#####	62.922	0.984	0.658	0.000	0.000	0.000	0.038	bdl	3.463
Massive ore	Average	38.253	51.547	877.479	47.983	0.357	430.100	######	60.944	634.654	18.196	#####	92.978	1.869	1.254	0.540	3.803	6.856	15.462	2.413	2.453
	Median	36.311	26.061	654.432	12.633	0.278	349.569	######	32.222	319.384	15.984	#####	82.129	2.294	1.126	0.157	0.347	1.548	2.603	0.087	1.281
	Std Dev	10.529	123.259	560.287	97.629	0.271	208.465	######	75.962	525.774	10.537	6.772	48.959	0.966	0.511	0.702	11.147	#####	43.886	4.726	3.350
	Maximum	75.872	641.701	#######	455.842	0.906	945.506	######	######	#######	32.525	#####	196.447	3.673	3.168	2.579	44.417	#####	######	15.588	16.343
	Minimum	24.207	12.193	498.037	bdl	0.013	247.326	######	0.291	165.048	4.121	#####	24.932	0.459	0.698	0.008	0.000	0.000	0.038	bdl	0.178
Skarn in Eastern contact zone	Average	708.370	464.064	#######	#######	######	#######	######	10.188	#######	21.975	3.428	998.428	#####	3.096	#####	12.863	#####	######	######	#######
	Median	693.729	467.502	#######	496.262	######	#######	######	8.565	#######	24.080	3.427	690.772	4.663	2.401	2.418	3.055	#####	######	69.880	#######
	Std Dev	148.708	28.368	503.022	#######	14.191	#######	######	7.513	#######	7.703	0.816	905.111	#####	2.046	#####	24.345	#####	######	######	#######
	Maximum	955.031	526.658	#######	#######	######	#######	######	28.049	#######	31.082	5.111	########	#####	8.702	#####	72.130	#####	######	######	#######
	Minimum	472.805	418.240	741.195	bdl	91.380	#######	######	3.083	#######	6.344	1.662	61.656	2.944	1.553	0.080	0.120	9.519	######	44.034	#######
N-BIF in Heinaobao	Average	270.642	#######	#######	74.607	0.120	317.707	37.681	45.903	328.539	4.654	6.532	79.305	5.034	6.469	0.724	0.132	1.136	0.651	0.177	2.022
	Median	122.573	#######	#######	0.000	0.093	307.192	37.605	43.030	331.629	4.465	6.969	70.342	4.891	6.508	0.802	0.076	0.795	0.584	0.140	1.997
	Std Dev	329.001	722.930	927.603	121.924	0.142	54.663	1.367	19.784	38.506	2.768	0.997	29.703	1.169	0.799	0.540	0.152	1.005	0.421	0.115	0.873
	Maximum	#######	#######	#######	295.979	0.429	401.605	41.108	79.836	383.893	7.732	8.109	146.150	6.399	7.562	1.638	0.406	3.007	1.392	0.358	3.758
	Minimum	45.429	581.206	702.572	bdl	bdl	244.097	36.233	17.794	272.302	1.837	5.215	53.010	3.583	5.139	0.109	bdl	0.212	0.139	0.056	0.609
G-BIF in Heinaobao	Average	164.595	#######	#######	248.691	2.428	#######	######	######	176.315	18.447	#####	255.023	#####	#####	0.028	0.012	0.333	3.301	1.716	6.994
	Median	152.734	#######	#######	241.721	2.409	#######	######	######	161.799	19.340	#####	245.408	#####	#####	0.034	0.007	0.334	2.682	1.782	6.476
	Std Dev	62.573	#######	327.953	44.218	0.338	382.781	6.167	73.432	41.409	1.834	2.993	46.941	5.037	1.180	0.020	0.013	0.081	1.287	0.434	1.640
	Maximum	332.632	#######	#######	295.979	2.882	#######	######	######	234.401	20.964	#####	354.182	#####	#####	0.053	0.039	0.501	5.553	2.331	9.745
	Minimum	103.156	#######	774.531	bdl	1.834	#######	######	35.322	122.335	15.576	#####	210.469	#####	9.714	bdl	bdl	0.232	2.008	1.016	4.965

	Item	Ba	La	Ce	Pr	Nd	Sm	Eu	Gd	Tb	Dy	Ho	Er	Tm	Yb	Lu	Hf	Ta	Bi	Pb
Disseminated ore	Average	11.887	2.936	5.050	0.594	2.052	0.317	0.095	0.233	0.064	0.445	0.082	0.245	0.027	0.160	0.016	0.014	0.006	0.053	1.446
	Median	3.688	0.129	0.389	0.054	0.184	0.106	0.028	0.070	0.016	0.141	0.022	0.034	0.006	0.046	0.008	0.015	0.006	0.040	0.398
	Std Dev	19.532	9.047	14.534	1.585	4.867	0.479	0.150	0.386	0.125	0.785	0.179	0.604	0.058	0.398	0.034	0.014	0.006	0.068	2.412
	Maximum	63.793	39.595	62.734	6.140	19.586	1.693	0.540	1.592	0.525	3.040	0.719	2.659	0.258	1.833	0.159	0.045	0.021	0.239	9.084
	Minimum	bdl	0.002	bdl	bdl	bdl	bdl	bdl	bdl	bdl	bdl	bdl	bdl	bdl	bdl	bdl	bdl	bdl	bdl	bdl
Banded ore	Average	0.970	1.055	3.826	0.484	2.386	0.458	0.137	0.332	0.068	0.551	0.113	0.331	0.039	0.216	0.028	0.068	0.003	0.064	1.084
	Median	0.294	0.093	0.745	0.071	0.480	0.101	0.019	0.060	0.013	0.056	0.013	0.040	0.010	0.030	0.006	0.011	0.001	0.010	0.147
	Std Dev	1.883	2.034	8.767	1.246	5.780	0.994	0.342	0.739	0.170	1.313	0.288	0.768	0.079	0.467	0.049	0.201	0.005	0.203	2.152
	Maximum	8.014	7.796	40.025	5.779	26.802	3.669	1.487	3.101	0.770	5.887	1.328	3.552	0.361	2.085	0.199	0.943	0.016	0.965	7.481
	Minimum	bdl	bdl	0.002	bdl	bdl	bdl	bdl	bdl	bdl	bdl	bdl	bdl	bdl	bdl	bdl	bdl	bdl	bdl	bdl
Massive ore	Average	27.895	5.036	10.245	0.922	4.135	1.058	0.351	0.965	0.183	1.250	0.223	0.809	0.068	0.274	0.029	0.398	0.059	0.191	0.492
	Median	3.306	0.388	1.324	0.148	0.513	0.126	0.031	0.127	0.010	0.144	0.020	0.045	0.004	0.016	0.005	0.074	0.006	0.017	0.230
	Std Dev	55.177	11.756	29.438	2.443	11.659	3.013	1.053	2.783	0.526	3.434	0.674	2.883	0.239	0.891	0.071	0.655	0.166	0.480	0.513
	Maximum	230.764	49.798	145.509	12.131	56.746	13.672	5.024	13.469	2.393	12.928	2.843	14.008	1.172	4.412	0.335	2.786	0.746	2.120	1.778
	Minimum	0.081	bdl	0.009	bdl	0.017	bdl	bdl	bdl	bdl	bdl	bdl	bdl	bdl	bdl	bdl	bdl	bdl	bdl	bdl
	Average	74.101	337.027	869.576	101.096	######	94.849	14.943	17.763	1.136	4.531	0.582	1.612	0.116	0.452	0.046	40.529	0.235	0.581	55.282
	Median	19.790	52.490	191.775	25.080	######	21.322	3.504	4.438	0.281	0.940	0.147	0.441	0.032	0.043	0.014	14.880	0.004	0.110	11.773

(*continued on next page*)

Table 1 (*continued*)

	Item	Mg	Al	Si	Ca	Sc	Ti	V	Cr	Mn	Co	Ni	Zn	Ga	Ge	Sr	Y	Zr	Nb	Mo	Sn
Skarn in Eastern contact zone	Std Dev	123.723	548.813	########	188.228	######	186.642	29.584	33.013	2.209	8.796	1.144	3.119	0.227	1.003	0.089	97.219	0.815	1.539	######	
	Maximum	403.752	########	########	614.391	######	605.908	96.739	######	7.006	27.586	3.387	9.093	0.714	3.268	0.321	######	3.064	5.864	######	
	Minimum	0.692	0.194	1.386	0.135	1.693	0.393	0.096	0.116	0.009	0.038	bdl	0.011	bdl	bdl	bdl	4.069	bdl	bdl	0.260	
N-BIF in Heinaobao	Average	1.182	0.016	0.023	0.003	0.025	0.034	0.011	0.032	0.004	0.035	0.014	0.026	0.009	0.041	0.002	0.060	0.031	0.048	0.548	
	Median	1.010	0.017	0.019	bdl	bdl	bdl	bdl	0.022	0.001	0.019	0.016	0.012	0.007	0.034	0.001	0.051	0.028	0.037	0.472	
	Std Dev	0.983	0.011	0.021	0.005	0.034	0.040	0.020	0.040	0.005	0.042	0.008	0.031	0.010	0.036	0.003	0.064	0.025	0.034	0.397	
	Maximum	3.339	0.033	0.059	0.014	0.079	0.100	0.057	0.121	0.012	0.106	0.028	0.076	0.029	0.098	0.008	0.207	0.093	0.114	1.183	
	Minimum	0.079	bdl	bdl	bdl	bdl	bdl	bdl	bdl	bdl	bdl	bdl	bdl	bdl	bdl	bdl	bdl	bdl	bdl	0.017	
G-BIF in Heinaobao	Average	0.276	0.153	0.318	0.028	0.102	0.023	0.015	0.029	0.004	0.005	0.008	0.022	0.003	0.015	0.004	0.065	0.546	0.003	0.224	
	Median	0.124	0.058	0.149	0.012	0.050	bdl	0.016	bdl	0.001	bdl	0.008	0.018	0.001	0.002	0.001	0.069	0.463	0.003	0.082	
	Std Dev	0.406	0.190	0.408	0.034	0.121	0.036	0.014	0.052	0.006	0.010	0.005	0.025	0.004	0.024	0.007	0.036	0.215	0.003	0.356	
	Maximum	1.341	0.581	1.235	0.093	0.376	0.097	0.034	0.146	0.016	0.032	0.015	0.078	0.012	0.071	0.020	0.116	0.982	0.007	1.164	
	Minimum	bdl	0.006	bdl	bdl	bdl	bdl	bdl	bdl	bdl	bdl	bdl	bdl	bdl	bdl	bdl	bdl	0.353	bdl	bdl	

Notes: Std Dev = standard deviation. bdl = below detection limit.

various magnetites. All spot analytical results of magnetite from Bayan Obo deposit, Eastern contact zone and Heinaobao are given in Table A1 and Table A2. The median values, mean values and standard deviations of trace element contents in magnetite are listed in Table 1.

5.1. Magnetite in three types of ores of Bayan Obo deposit

In general, the three types of magnetite in Bayan Obo deposit show similar trace element contents, REE distribution patterns and trace element patterns (Figs. 5-9). The contents of Ni (~50–100 ppm) of three are the highest in all types of magnetites (Figs. 5d; 6), but the contents of Mg (22–133 ppm), Al (7–640 ppm), Ti (102–945 ppm), Mn (165–1900 ppm), Zn (25–350 ppm), Ga (0.5–3.6 ppm) and Ge (0.6–3.2 ppm) are lower than those in skarn in the Eastern contact zone and BIF at Heinaobao (Figs. 5a-e; 6). In addition, the magnetite in the Bayan Obo deposit exhibits a large variation in terms of trace elemental concentrations, such as Mg (22–195 ppm), V (38–1200 ppm), Y (<0.01–45 ppm), Nb (0.04–210 ppm), Sc (0.01–35 ppm), REE (0.1–280 ppm; Fig. 5a, b, e, f, h), which are similar to the magnetite formed in hydrothermal environment (Nadoll et al., 2014). Compared with magnetites in the skarn and BIF, the three types of magnetites in the Bayan Obo deposit have very low Ti/V and Al/Co ratios (Fig. 7a, e), and the Zn/V, Zr/Hf, Nb/Ta, La/Yb and Ti/Al ratios vary greatly (Fig. 7b, d-f). In the multi-element diagram, the three types of magnetites in the Bayan Obo deposit show positive anomalies of Mg, Si and Nb, and negative anomalies of Ti, Al and Cr (Fig. 8a-c), which are obviously different from the magnetite from Skarn in Eastern contact zone and BIF in Heinaobao. The magnetite from Bayan Obo has a weak LREE enrichment (Fig. 9), which is completely different from the strong enrichment of LREE in magnetite of skarn and the depletion of LREE in magnetite of N-BIF. The total REE contents of magnetite from Bayan Obo are significantly higher than that of magnetite in BIF, but the LREE contents are significantly lower than that of magnetite in skarn.

The contents of some trace elements are significantly different in magnetite from different samples of the same kind of ore. The two banded ores (17BY164, 17BY206) analyzed in this study show obviously different contents of V, Ti, Ge, Ni and Co (Fig. 5b-d, g), while the three massive ores (17BY60, 17BY81 and 17BY190) also have different contents of V, Mn and Co (Fig. 5b, c, g). This is consistent with the trace element data of magnetite obtained by Huang et al. (2015).

5.2. Magnetite in skarn of Eastern contact zone

Magnetite in the skarn of the Eastern contact zone has the highest contents of Mg (470–950 ppm), Ti (44000–59000 ppm), Mn (20500–34900 ppm), Sc (90–150 ppm), Zn (60–2430 ppm), Nb (210–2850 ppm) and REE (4–11500 ppm) and the lowest content of Ni (1.7–5.1 ppm) in all types of magnetite (Figs. 5; 6), and the ratios of Sn/Ga, Co/Ni, Nb/Ta, La/Yb, Ti/V and Ti/Al are also the highest (Fig. 7a, b, d-f). Compared with the three types of magnetite in Bayan Obo deposit, the magnetite in skarn shows weak negative anomalies of Al and Si, and positive anomalies of Ti and Pb (Fig. 8d), strong enrichment in LREE and the highest total REE contents (Fig. 9). As a whole, the trace element contents of magnetite in skarn of Eastern contact zone are generally high and variable, which is consistent with the high temperature environment of endoskarn.

5.3. Magnetite in BIF of Heinaobao

Magnetite grains from the N-BIF have the lowest V (36–41 ppm), Nb (0.14–1.4 ppm), Sc (0.03–0.43 ppm), Co (1.8–7.7 ppm) and REE contents (0.20–0.34 ppm; Figs. 5b, f-h; 6), and medium content of Al (580–2810 ppm), Ga (3.6–6.4 ppm), Ge (5.1–7.6 ppm) and Ni (5.2–8.1 ppm) (Fig. 5a, c, d), while magnetite from the G-BIF has the highest content of Al (7610–12000 ppm), Ga (32–46 ppm) and Ge (9–13 ppm) (Figs. 5a, c, d; 6), medium contents of Ti (4400–5450 ppm), Zn

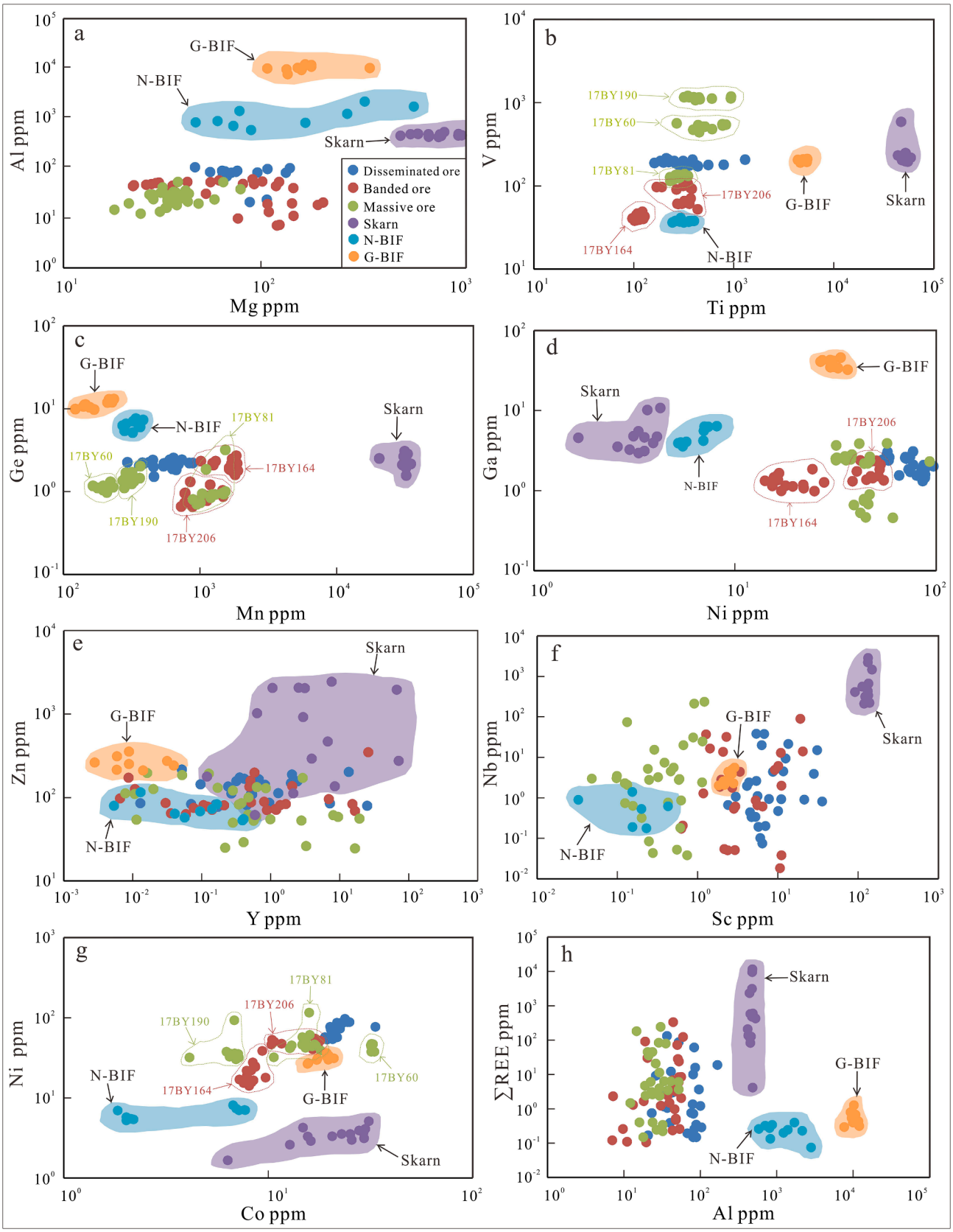

Fig. 5. Bi-modal plots of Al vs. Mg, V vs. Ti, Ge vs. Mn, Ga vs. Ni, Zn vs. Y, Nb vs. Sc, Ni vs. Co, and ∑REE vs. Al in magnetite from disseminated ore, banded ore and massive ore in the Bayan Obo deposit, skarn in the Eastern Contact Zone and BIF-type ore in Heinaobao.

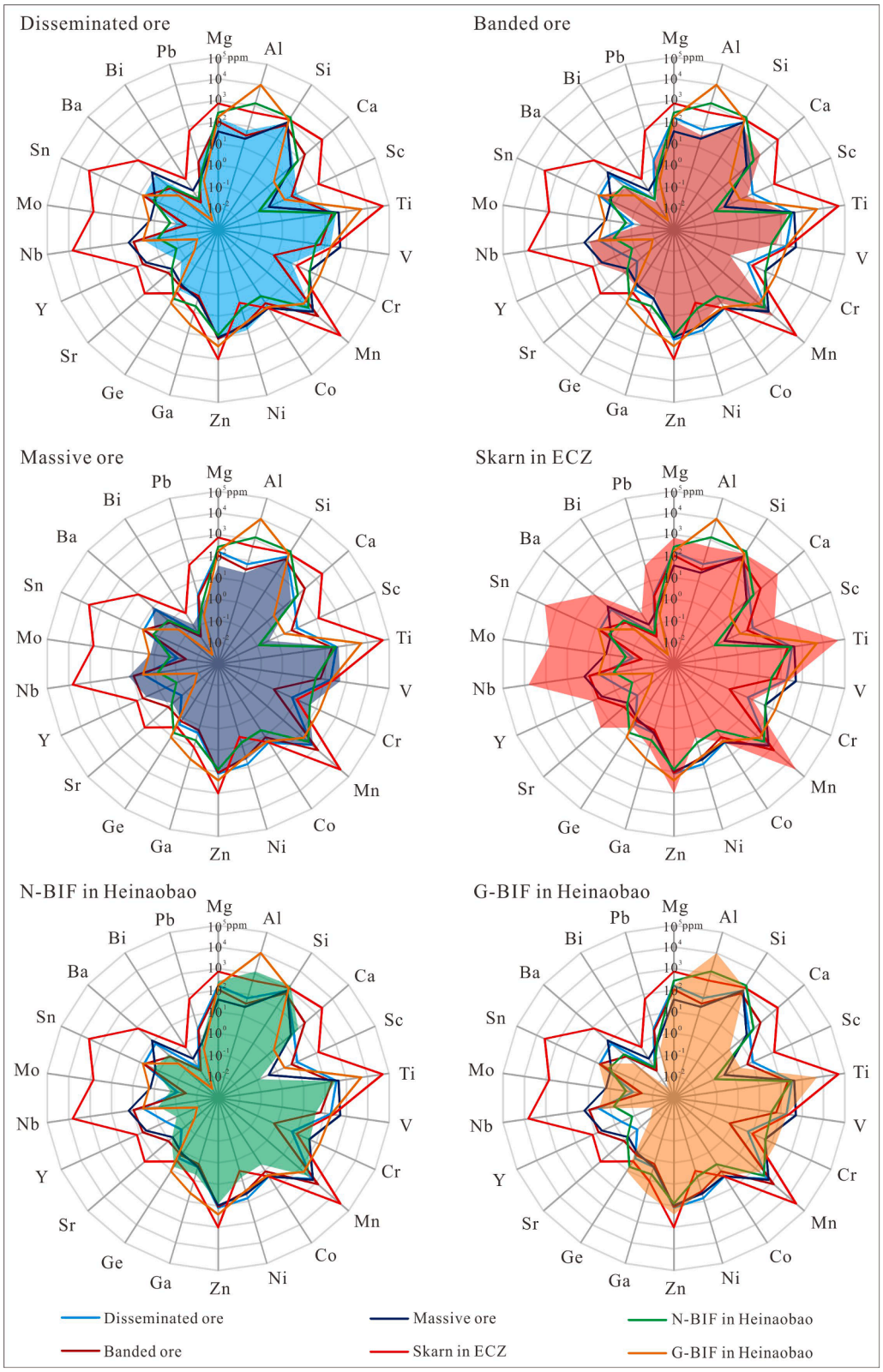

Fig. 6. Radar plots of mean values, in parts per million, for trace elements in magnetite from disseminated ore, banded ore and massive ore in the Bayan Obo deposit, skarn in the Eastern Contact Zone (ECZ) and BIF-type ore in Heinaobao.

(210–354 ppm), Nb (2–5.5 ppm) and Sc (1.8–2.9 ppm), and the lowest REE (0.10–0.42 ppm), Mn (122–235 ppm), Sr (<0.05 ppm) and Y (<0.04 ppm) content (Figs. 5; 6). The magnetite in the Heinaobao BIF has the lowest Nb/Ta, Ti/Al and Sn/Ga ratios, and the highest Al/Co ratio (Fig. 7a, d, f). In contrast to magnetite in the Bayan Obo deposit, magnetite from the Heinaobao BIF shows negative Mg anomaly, positive Al and Ti anomalies, and weak negative anomalies of Nb and Cr (Fig. 8e). Magnetite in N-BIF has an obvious depletion of light rare earth,

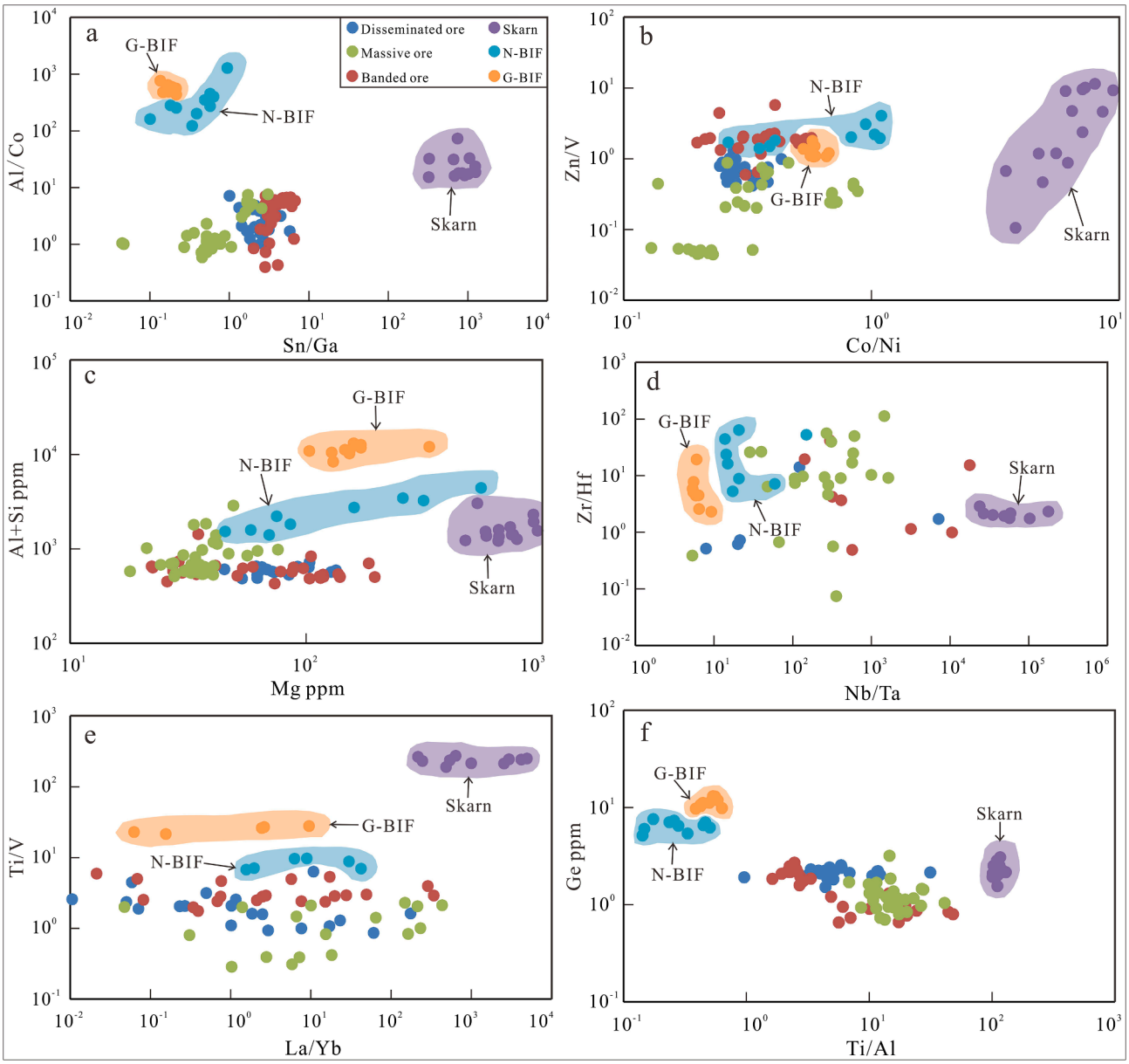

Fig. 7. Scatter diagrams of trace elements for different types of magnetites in the Bayan Obo deposit, the Eastern Contact Zone, and Heinaobao. a: Al/Co vs. Sn/Ga; b: Zn/V vs. Co/Ni; c: (Al + Si) vs. Mg; d: Zr/Hf vs. Nb/Ta; e: Ti/V vs. La/Yb; f: Ge vs. Ti/Al.

La positive anomaly and weak Ce negative anomaly, while magnetite in the G-BIF is relatively enriched in light rare earth with weak Ce and Eu positive anomalies (Fig. 9). The REE contents of magnetite in the two BIF are significantly lower than that of skarn in the Eastern contact zone and the ores in Bayan Obo (Figs. 5h; 9).

6. Discussion

6.1. Nature of different types of magnetite

6.1.1. Magnetite in the Bayan Obo iron ores

The Mesoproterozoic iron-mineralization event in Bayan Obo can be divided into three stages from the early to the late, namely, the disseminated, the banded and the massive mineralization respectively (Liu et al., 2018a), which are corresponding to three types of iron ores collected from Bayan Obo in this study. The trace element concentrations of Bayan Obo magnetite are generally lower than those of magmatic magnetite from global igneous carbonatites, except for REEs (Gaspar and Wyllie, 1983; Reguir et al., 2008; Milani et al., 2017; Ranta et al., 2018; Chen et al., 2019). In contrast to the hydrothermal magnetite associated with igneous carbonatite, such as those in Hongcheo and Phalaborwa, magnetite from Bayan Obo is enriched in Ti, V, Mn, Zn, Nb and REE, and depleted in Mg, Al, Sc, Co (10–21 ppm) and Ni (40–71 ppm; Milani et al., 2017; Chen et al., 2019).

Co-existing mineral phases, such as silicates and sulfides, significantly affect the concentration of trace elements in magnetite (Gaetani and Grove, 1997; Carew, 2004; Simon et al., 2008; Schilling et al., 2011; Nadoll et al., 2014; Chen et al., 2015; Huang et al., 2019b). Magnesium, Al and Ti tend to participate into mafic silicate minerals (Frost, 1991; Toplis and Corgne, 2002; Simon et al., 2008), so these elements in magnetite were always depleted. Similar results were found in the Bayan Obo in this study. The silicate minerals associated with magnetite, namely aegirine and riebeckite, are extremely enriched in Mg (5000–80,000 ppm), Al (3000 ppm), Ti (1000–6000 ppm) and V (300–1000 ppm; Liu et al., 2018c). Hence, both silicate minerals are the main factors causing the depletion of Mg, Al, Ti and V in Bayan Obo

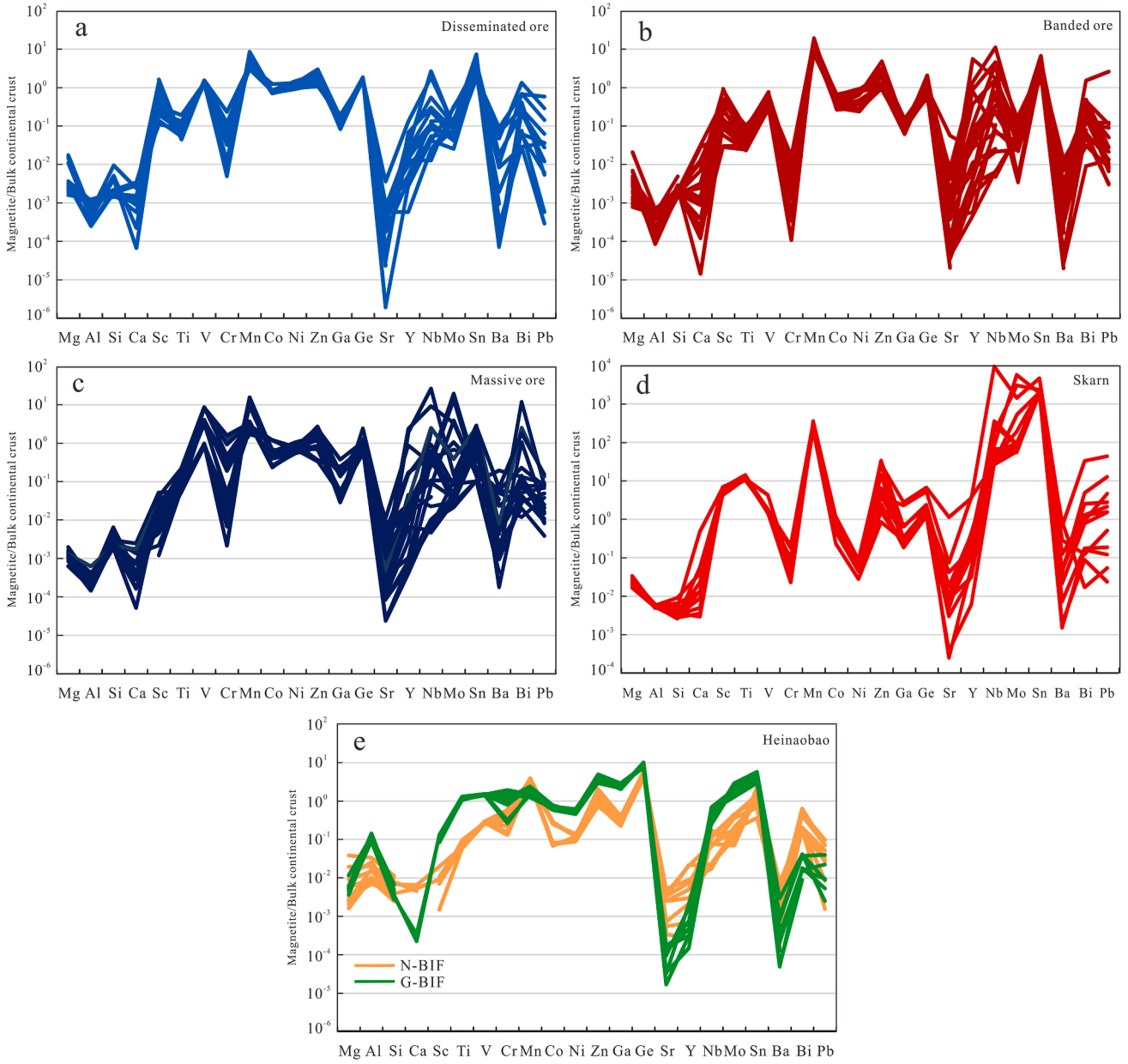

Fig. 8. Normalized multi-elemental patterns of magnetite for a: disseminated ore, b: banded ore and c: massive ore in the Bayan Obo deposit, d: skarn in the Eastern contact zone and e: BIF-type ore in Heinaobao. Trace element contents of bulk continental crust are from Rudnick and Gao (2003).

magnetite. Compared with Hongcheo and Phalaborwa magnetite, Bayan Obo magnetite has relatively high and uniform Ti and Zn contents indicating a higher and constant temperature of precipitation (Lindsley, 1991; Nielsen et al., 1994; Nielsen and Beard, 2000; Toplis and Corgne, 2002; Nadoll et al., 2014, 2015; Milani et al., 2017). Elements with various valence in magnetite, such as V and Mn, are closely related to oxygen fugacity. With the increase of oxygen fugacity, the compatibility of V and Mn decreased and increased respectively (Toplis and Corgne, 2002; Reguir et al., 2008; Bordage et al., 2011; Nadoll et al., 2014). From disseminated ore, through banded ore, to massive ore, the V content in magnetite firstly decreases and then increases, while the Mn content firstly increases and then decreases (Table 1). The negative correlation between V and Mn in the magnetite indicates that Mn content in Bayan Obo magnetite is controlled by oxygen fugacity, while V content is jointly controlled by oxygen fugacity and silicate minerals. The difference of V and Mn in magnetite of different samples in the same type of ore indicates different redox environments. Nickel, Co and Cr in Bayan Obo magnetite are presented with very low concentrations, but they are compatible elements in magnetite (Righter et al., 2006; Ranta et al., 2018), indicating the scarcity of Cr, Ni and Co in the hydrothermal system of magnetite crystallization. The distribution coefficient of rare earth elements and niobium between magnetite and melt/fluid is low (Dare et al., 2012; Huang et al., 2015). Therefore, the low content of REEs and Nb in magnetite also indicate that the concentrations of these elements in the ore-forming fluid are high, which is corresponding to the large distribution of rare earth minerals and niobium-bearing minerals in different ores of Bayan Obo (Fan et al., 2016; Liu et al., 2018a).

6.1.2. *Magnetite in skarn of the Eastern contact zone*

Compared to magnetite in other skarns such as those in Ertsberg district, Chengchao and Tieshan deposits (Nadoll et al., 2014; Wang et al., 2017; Li et al., 2019; Dong et al., 2021), the skarn magnetite in the Eastern contact zone has dramatically high Sc, Ti, Mn, Zn, Nb, REE, Mo (44–4514 ppm), and Sn (3127–7835 ppm), but low Mg (473–955 ppm)

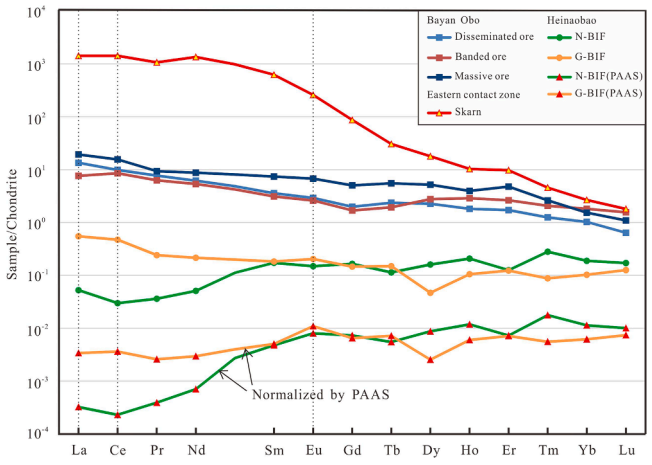

Fig. 9. Chondrite-normalized rare-earth-element patterns (mean value) of magnetite from different types of ores from Bayan Obo, Eastern contact zone and Heinaobao. The values of rare earth elements used in this figure are average. Rare earth element contents of chondrite and Post-Archean Australian average shale (PAAS) are from Sun and McDonough (1989) and McLennan (1989), respectively.

and V (195–590 ppm). The trace elements compositions of Bayan Obo granites show that the contents of Mn, Nb and REE were 310–850 ppm, 12–24 ppm, 330–540 ppm, respectively (Ling et al., 2014), while the contents of the three in the ore-hosting dolomite were 4027–23234 ppm, 24–650 ppm, 15000–45000 ppm, respectively (Yang et al., 2011), indicating that the high contents of Mn, Nb and REE of skarn magnetite came from ore-hosting dolomite rather than granite. In addition, the similar trace elements and REE distribution patterns between ore-hosting dolomite and skarn magnetite also confirm this standpoint. Consequently, the extremely high and variable Mn, Nb and REE contents of magnetite in skarn of the Eastern contact zone may be controlled by the participation degree of ore-bearing dolomite in skarn mineralization. The skarn samples used in this study were collected from endoskarn zone with high forming temperature (590–770 °C; Ling et al., 2014), which may be an important factor for the extreme enrichment of Ti and Sn in skarn magnetite (Nielsen et al., 1994; McQueen and Cross, 1998; Nadoll et al., 2012; Dare et al., 2014). Compared with magnetite, its associated pyrite has high Co (320–563 ppm) and Ni (24–123 ppm) and low Sc (<0.36 ppm) and Zn (<3.2 ppm; unpublished data), therefore, the enrichment of Sc, Zn and depletion of Co, Ni in magnetite may be caused by the preferentially participation of these trace elements between magnetite and sulfide (Huang et al., 2014; Nadoll et al., 2014; Chen et al., 2015). The low V content indicates that the magnetite in the skarn of the Eastern contact zone was formed under higher oxygen fugacity than those in the skarn of Ertsberg district (Toplis and Corgne, 2002; Ryabchikov and Kogarko, 2006; Reguir et al., 2008; Nadoll et al., 2014).

6.1.3. Magnetite in the Heinaobao BIF

Compared with typical BIF magnetite in the world, the magnetite in N-BIF is enriched in Al, Ti, V, Cr, Mn, and Zn, depleted in Mg, and Sc, and have similar Co, Ni, Ga, and Nb, while the magnetite in G-BIF is enriched in Al, Sc, Ti, V, Cr, Mn, Co, Ni, Zn, Ga, and Nb and depleted in Mg (Angerer et al., 2012; Nadoll et al., 2014; Gourcerol et al., 2016). In addition to mineral compositions, there are significant differences in the geochemical composition of magnetite of both BIFs in Heinaobao. Compared with the magnetite in N-BIF, those in G-BIF have higher contents of Al, Sc, Ti, V, Cr, Co, Ni, Zn, Ga, Nb and REE, but lower Si, Fe, Mn, Sr, Y and Ba (Table 1; Figs. 5, 8e, 9). Magnetite in G-BIF shows positive Eu anomaly, weak LREE enrichment in Chondrite-normalized REE patterns, but sub-parallel REE patterns normalized by Post-Archean Australian Shale. Magnetite in N-BIF was characterized by LREE depletion coupled with positive La and Eu anomalies, and negative Ce anomalies in both normalized REE patterns, which is consistent with the characteristics of REEs in BIF all over the world (Fig. 9; Angerer et al., 2012; Liu et al., 2014; Gourcerol et al., 2016; Moon et al., 2017; Ebotehouna et al., 2021; Tamehe et al., 2021). The weak Eu and Ce anomalies indicate a lower redox level during syngenetic deposition (Liu et al., 2014). The same sedimentary environment, and the main factors controlling the composition of magnetite in BIFs (seawater composition, temperature and oxygen fugacity; Nadoll et al., 2014; Ebotehouna et al., 2021) are similar. Large amounts of Al-rich minerals in G-BIF, such as garnet and plagioclase, indicate that the contamination of terrigenous detrital material may be the most appropriate explanation for the difference in mineral composition and magnetite geochemical composition of the two BIFs in Heinaobao (Haugaard et al., 2013; Gourcerol et al., 2016; Ndime et al., 2019; Tamehe et al., 2021). This view can be supported by the trace elements of magnetite, that is, compared with magnetite in N-BIF, G-BIF magnetite has 1) higher content of Al, Sc, Ti, Ga, Nb, transition metals and REE, and depletion in Fe, Si, Mg; 2) enrichment of LREE and low Y/Ho; 3) a slight positive correlation between Al, Ti and other trace elements (Haugaard et al., 2013; Viehmann et al., 2015; Moon et al., 2017; Ndime et al., 2019; Tamehe et al., 2021). From the above, we propose that N-BIF of Heinaobao is detritus-free, whereas G-BIF has a significant amount of clastic material. Similar results were recently reported in Sanheming in the southeast and Gongjucheng in the south of Heinaobao deposit, Nkout West and Bikoula BIF in southern Cameroon, and Itilliarsuk BIF in West Greenland (Haugaard et al., 2013; Nan et al., 2017; Teutsong et al., 2017; Ndime et al., 2019).

6.2. Is Bayan Obo a skarn or BIF type iron deposit?

Recent studies have confirmed that magnetite trace elements obtained by LA-ICP-MS can reflect different types of mineralization or fluid evolution, and therefore a large number of discrimination diagrams have been established to identify magnetite formed from various ore-forming environments, or different types of ore deposits (Singoyi et al., 2006; Beaudoin and Dupuis, 2009; Rusk et al., 2010; Dupuis and Beaudoin, 2011; Dare et al., 2012; Nadoll et al., 2014; Knipping et al., 2015; Chen et al., 2019; Aftabi et al., 2021). The main ore mineral, magnetite, of the Bayan Obo deposit, thus provides an opportunity to study the origin of the deposit.

In the diagrams of Ni/(Cr + Mn) vs. Ti + V and Ca + Al + Mn vs. Ti + V (Fig. 10a, b), the three types of magnetite in Bayan Obo plot in the field for skarn and IOCG deposits, and some of them fall into the BIF field. The extremely high Ti and Al content causes the magnetite in skarn to plot in the field of magmatic Fe-Ti-oxide deposits. The two types of BIF magnetite in Heinaobao fall outside the field of typical BIF deposit. The magnetite enriched in Cr and Mn in N-BIF fall into the field for skarn deposit, while those enriched in Ti and Al in G-BIF fall between skarn and porphyry deposit. Hence, the two discrimination diagrams have disadvantages in distinguishing between terrigenous material contaminated BIF and skarn/porphyry deposit. Although there is a small overlap in the Ca + Al + Mn vs. Ti + V diagram between the magnetite in the Bayan Obo banded ore and the magnetite in the N-BIF of Heinaobao (Fig. 10b), it is due to the anomalous contents of Al, Cr and Mn in magnetite of N-BIF. Recently, many researches have documented similar situations in which magnetites from typical skarn, IOCG, IOA and BIF deposits do not fall into the expected zones (Hu et al., 2014; Nadoll et al., 2014; Chen et al., 2015; Chung et al., 2015; Knipping et al., 2015; Gourcerol et al., 2016; Huang et al., 2019b), which shows that these discrimination diagrams are not always reliable and lead to misclassification of samples. We consider that it is meaningful to use discriminant diagrams to identify deposits or rocks only when the mineralogical characteristics of the samples and the magmatic/fluid chemical properties of magnetite precipitation are clear, and multiple discriminant diagrams should be used together.

The trace element content of magnetite obtained in the present study

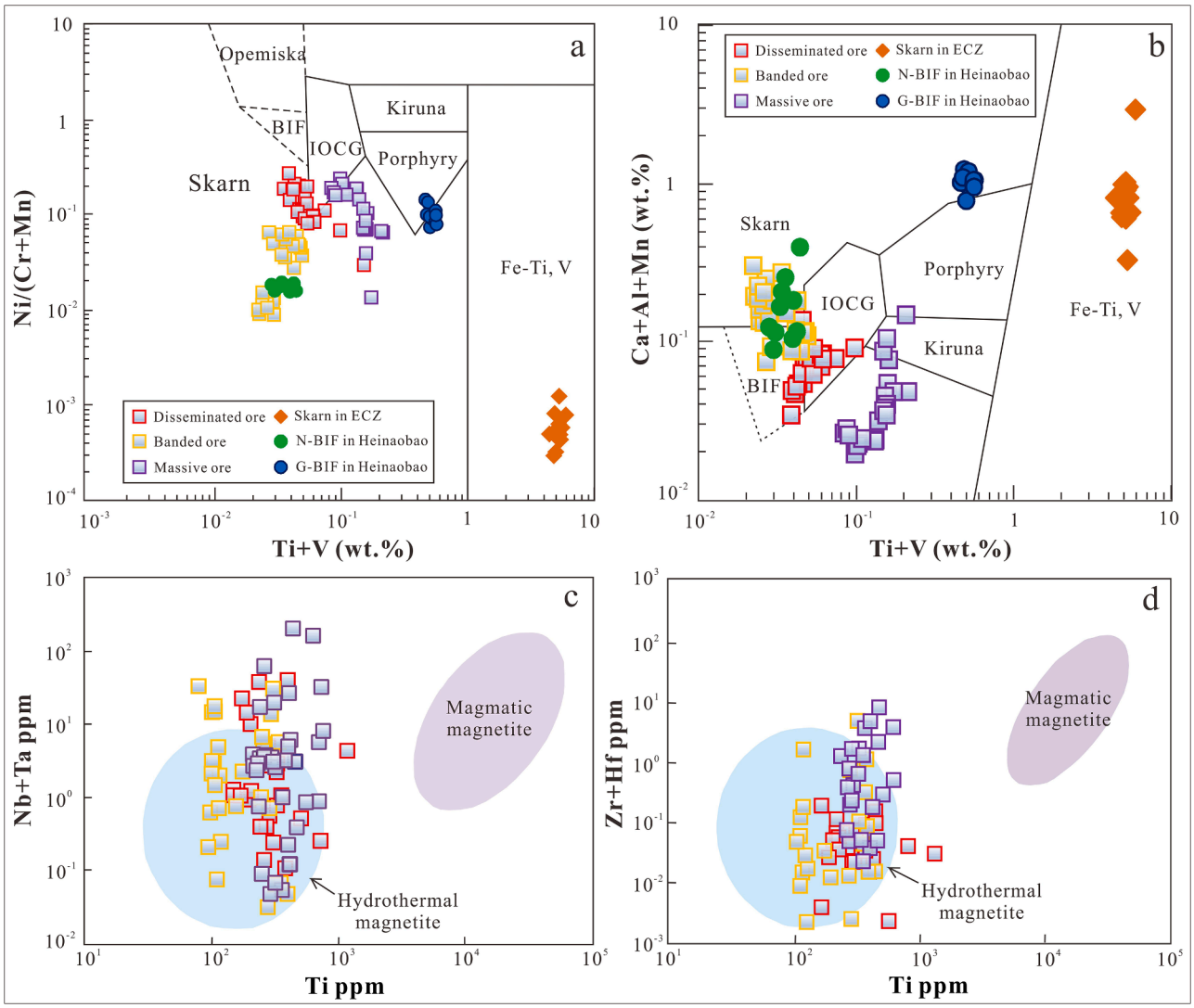

Fig. 10. a, b: plots of Ni/(Cr + Mn) vs. Ti + V and Ca + Al + Mn vs. Ti + V of magnetite from the Bayan Obo deposit, the Eastern contact zone (ECZ) and Heinaobao. Reference fields are after Dupuis and Beaudoin (2011). BIF: banded iron formation; Skarn: Fe-Cu skarn deposits; IOCG: iron oxide-copper-gold deposits; Porphyry: porphyry Cu deposits; Kiruna: Kiruna apatite-magnetite deposits; Fe–Ti, V: magmatic Fe-Ti-oxide deposits. c, d: plots of Ti vs Nb + Ta and Ti vs. Zr + Hf to distinguish magmatic and hydrothermal magnetite. The reference fields of magmatic and hydrothermal magnetite associated with carbonatite is from Chen et al. (2019).

indicates that the Bayan Obo magnetite has the highest Ni, but the Mg, Al, Ti, Ge, Mn, Ga and Zn contents are all lower than those in skarn of Eastern contact zone and BIF of Heinaobao (Fig. 5). In binary diagrams of elemental ratio (Fig. 7), the Bayan Obo magnetite has no overlap with the magnetite in skarn and BIF. In addition, the distribution patterns of trace elements (Fig. 8) and rare earth elements (Fig. 9) in Bayan Obo magnetite are also different from those of skarn and BIF. Compared with magmatic magnetite in carbonatite, the magnetites in Bayan Obo generally lack high field strength elements, such as Zr, Hf and Ta (Fig. 10c, d), and have strong positive Mn and Zn anomalies and negative Co and Ga anomalies, which are similar to hydrothermal magnetite associated with carbonatite (Table 1; Fig. 8a-c; Chen et al., 2019). Chen et al. (2019) proposed that the discrimination diagrams of Ti vs. Zr + Hf and Ti vs. Nb + Ta could be used to distinguish magmatic magnetite from hydrothermal magnetite in carbonatite-related environments, and the hydrothermal magnetite associated with carbonatite has low Ti (<1000 ppm), Zr + Hf and Nb + Ta (<10 ppm). Except for magnetite with anomalous content of Nb and Zr, most of the Bayan Obo magnetite falls into the field of hydrothermal magnetite associated with igneous carbonatite in both diagrams, but all of them are outside the field of magmatic magnetite (Fig. 10c, d). In general, the magnetites in Bayan Obo generally show low and variable trace element compositions, most of which keep similar characteristics to magnetites formed in hydrothermal environment (Nadoll et al., 2014, 2015). Based on the above, we believe that the Bayan Obo iron deposit is a hydrothermal deposit related to igneous carbonatite, instead of skarn Fe- or BIF deposit.

7. Conclusions

The trace element contents of three types of magnetite in Bayan Obo REE-Nb-Fe deposit are generally low and vary widely, which are similar to that of magnetite precipitated in hydrothermal environment. Co-existing silicate minerals, such as aegirine and riebeckite, caused magnetite of Bayan Obo to be extremely depleted in Mg, Al, Ti and V. The negative correlation between V and Mn indicates that the distribution of V and Mn in magnetite is mainly controlled by oxygen fugacity. Compared with magnetite in BIF of Heinaobao and skarn of Eastern contact zone, the Bayan Obo magnetite is rich in Ni, but depleted in Mg, Al, Ti, Ge, Mn, Ga, Zn. Moreover, the ratio of trace elements and the distribution pattern of rare earth and trace elements in Bayan Obo magnetite are completely different from those in Heinaobao and Eastern contact zone, but similar to the hydrothermal magnetite related to the

igneous carbonatite. Hence, we propose that the iron resources at Bayan Obo REE-Nb-Fe deposit is of hydrothermal origin related to igneous carbonatite, neither formed as BIF nor skarn deposit. In this study, both skarn magnetite formed at high temperature and BIF magnetite contaminated with terrigenous material have deviated from the expected filed in the diagrams of Ni/(Cr + Mn) vs. Ti + V and Ca + Al + Mn vs. Ti + V. Our work is very consistent with previous studies that discrimination diagrams are useful to identify deposits or rocks only if mineralogical characteristics of the samples and magmatic/fluid chemistry of magnetite precipitation are clear, and that multiple discrimination diagrams are required in combination.

Declaration of Competing Interest

The authors declare that they have no known competing financial interests or personal relationships that could have appeared to influence the work reported in this paper.

Acknowledgements

We sincerely thank Er-Dou Li, Qiang Li, Zhang Liu, Hai-Long Jin and Zhen-Jiang Wang of Baotou Rare Earth Research Institute for their helps during the field work, and Ms. Xue Zhang of State Key Laboratory of Ore Deposit Geochemistry (IGCAS) and Mr. Guang-Yu Shi of Wuhan Sample Solution Analytical Technology Co., Ltd, Hubei, China for their technical support in trace and major element analyses of magnetite. Two anonymous reviewers are thanked for their constructive comments, which improved the quality of this manuscript. This work is funded by the National Natural Science Foundation of China (41930430, 91962103), the Key Research Program of the Institute of Geology and Geophysics, CAS (IGGCAS-201901), and the Opening Project of the State Key Laboratory of Baiyunobo Rare Earth Resource Researches and Comprehensive Utilization (2021H2280).

Appendix A. Supplementary data

Supplementary data to this article can be found online at https://doi.org/10.1016/j.oregeorev.2021.104574.

References

Aftabi, A., Atapour, H., Mohseni, S., Babaki, A., 2021. Geochemical discrimination among different types of banded iron formations (BIFs): A comparative review. Ore Geol. Rev. 136.

Angerer, T., Hagemann, S.G., Danyushevsky, L.V., 2012. Geochemical evolution of the banded iron formation-hosted high-grade iron ore system in the Koolyanobbing Greenstone Belt, Western Australian. Econ. Geol. 107, 599–644.

Bai, G., Yuan, Z.X., Wu, C.Y., Zhang, Z.Q., Zheng, L.X., 1996. Demonstration on the Geological Features and Genesis of the Bayan Obo Ore Deposit. Geological Publishing House, Beijing (in Chinese).

Barnes, S.J., Roeder, P.L., 2001. The range of spinel composition in terrestrial mafic and ultramafic rocks. J. Petrol. 42, 2279–2302.

Beaudoin, G., Dupuis, C., 2009. Iron-oxide trace element fingerprinting of mineral deposit types. In: Mumin, A.H., Corriveau, L. (Eds.), Exploring for iron oxide copper-gold deposits: Canada and global analogues. GAC Short Course Notes, pp. 107–121.

Bordage, A., Baland, E., Villiers, J.R., Cromarty, R., Juhim, A., Carvallo, C., Calas, G., Sunder Raju, P.V., Glatzel, P., 2011. V oxidation state in Fe–Ti oxides by high-energy resolution fluorescence-detected X-ray absorption spectroscopy. Phys. Chem. Miner. 38, 449–458.

Campbell, L.S., Compston, W., Sircombe, K.N., Wilkinson, C.C., 2014. Zircon from the East Orebody of the Bayan Obo Fe–Nb–REE deposit, China, and SHRIMP ages for carbonatite-related magmatism and REE mineralization events. Contrib. Mineral. Petrol. 168, 1–23.

Campbell, L.S., Henderson, P., 1997. Apatite paragenesis in the Bayan Obo REE-Nb-Fe ore deposit, Inner Mongolia, China. Lithos 42, 89–103.

Cao, R.L., Zhu, S.H., Wang, J.W., 1994. Source materials for the Bayan Obo Fe-REE ore deposit and problems on the genetic theory. Sci, China (Series B) 24, 1298–1307 (in Chinese).

Carew, M.J., 2004. Controls on Cu-Au Mineralisation and Fe Oxide Metasomatism in the Eastern Fold Belt, NW Queensland, Australia. James Cook University (Ph. D thesis), Queensland, pp. 213–277.

Carew, M.J., Mark, G, Oliver, N.H.S., Pearson, N., 2006. Trace element geochemistry of magnetite and pyrite in Fe oxide (±Cu-Au) mineralised systems: Insights into the geochemistry of ore-forming fluids. Geochim. Cosmochim. Acta 70, A83-A83.

Chao, E.C.T., Back, J.M., Minkin, J.A., Tatsumoto, M., Wang, J.W., Conrad, J.E., MaKee, E.H., Hou, Z.L., Meng, Q.R., Huang, S.G., 1997. The sedimentary carbonate-hosted giant Bayan Obo REE-Fe-Nb ore deposit of Inner Mongolia, China: a cornerstone example for giant polymetallic ore deposits of hydrothermal origin. US Geol. Surv. Bull. 2143, 1–65.

Chao, E.C.T., Tatsumoto, M., Minkin, J.A., Back, J.M., Mckee, E.H., Ren, Y.C., Li, G.M., 1991. Muitiple lines of evidence for establishing the mineral paragenetic sequence of the Bayan Obo rare earth ore deposit of Inner Mongolia, China. Contr. Geol. Miner. Resour. Res. 6, 1–17 (in Chinese with English abstract).

Chen, W., Ying, Y.C., Bai, T., Zhang, J.J., Jiang, S.Y., Zhao, K.D., Shin, D., Kynicky, J., 2019. In situ major and trace element analysis of magnetite from carbonatite-related complexes: Implications for petrogenesis and ore genesis. Ore Geol. Rev. 107, 30–40.

Chen, W., Liu, H.Y., Lu, J., Jiang, S.Y., Simonetti, A., Xu, C., Zhang, W., 2020. The formation of the ore-bearing dolomite marble from the giant Bayan Obo REE-Nb-Fe deposit, Inner Mongolia: insights from micron-scale geochemical data. Miner. Deposita. 55, 131–146.

Chen, W.T., Zhou, M.-F., Li, X., Gao, J.F., Hou, K., 2015. In-situ LA-ICP-MS trace elemental analyses of magnetite: Cu-(Au, Fe) deposits in the Khetri copper belt in Rajasthan Province, NW India. Ore Geol. Rev. 65, 929–939.

Chung, D., Zhou, M.F., Gao, J.F., Chen, W.T., 2015. In-situ LA-ICP-MS trace elemental analyses of magnetite: The late Paleoproterozoic Sokoman Iron Formation in the Labrador Trough, Canada. Ore Geol. Rev. 65, 917–928.

Dare, S.A.S., Barnes, S.J., Beaudoin, G., Meric, J., Boutroy, E., Potvin-Doucet, C., 2014. Trace elements in magnetite as petrogenetic indicators. Miner. Deposita. 9, 785–796.

Dare, S.A.S., Barnes, S.J., Beaudoin, G., 2012. Variation in trace element contents of magnetite crystallized from a fractionating sulphide liquid, Sudbury, Canada: implications for provenance discrimination. Geochim. Cosmochim. Acta 88, 27–50.

Dong, R., Wang, H., Li, W.Q., Yan, Q.H., Zhang, X.Y., 2021. The geology, magnetite geochemistry, and oxygen isotopic composition of the Akesayi skarn iron deposit, Western Kunlun Orogenic Belt, Xinjiang, northwest China: Implications for ore genesis. Ore Geol. Rev. 130.

Drew, L.J., Meng, Q.R., Sun, W.J., 1990. The Bayan Obo iron-rare earth-niobium deposits, Inner Mongolia, China. Lithos 26, 43–65.

Dupuis, C., Beaudoin, G., 2011. Discriminant diagrams for iron oxide trace element fingerprinting of mineral deposit types. Miner. Deposita. 46, 319–335.

Duran, C.J., Barnes, S.J., Mansur, E.T., Dare, S.A.S., Bedard, L.P., Sluzhenikin, S.F., 2020. Magnetite chemistry by LA-ICP-MS records sulfide fractional crystallization in massive nickel-copper-platinum group element ores from the Norilsk-Talnakh mining district (Siberia, Russia): implications for trace element partitioning into magnetite. Econ. Geol. 115, 1245–1266.

Ebotehouna, C.G., Xie, Y.L., Adomako-Ansah, K., Gourcerol, B., Qu, Y.W., 2021. Depositional environment and genesis of the Nabeba Banded Iron Formation (BIF) in the Ivindo Basement Complex, Republic of the Congo: perspective from whole-rock and magnetite geochemistry. Minerals 11, 579.

Fan, H.R., Hu, F.F., Yang, K.F., Wang, K.Y., 2006. Intrusive age of No.1 carbonatite dyke from Bayan Obo REE-Nb-Fe deposit, Inner Mongolia: with answers to comment of Dr. Le Bas. Acta Petrol. Sinica 22, 519–520 (in Chinese with English Abstract).

Fan, H.R., Hu, F.F., Yang, K.F., Wang, K.Y., Liu, Y.S., 2009. Geochronology framework of late Paleozoic dioritic-granitic plutons in the Bayan Obo area, Inner Mongolia, and tectonic significance. Acta Petrol. Sinica 25, 2933–2938 (in Chinese with English abstract).

Fan, H.R., Xie, Y.H., Wang, K.Y., 2002. Fluid inclusions in skarn in eastern contacting zone of Bayan Obo REE-Nb-Fe deposit. Miner. Deposits. 21, 808–811 (in Chinese with English abstract).

Fan, H.R., Yang, K.F., Hu, F.F., Liu, S., Wang, K.Y., 2016. The giant Bayan Obo REE-Nb-Fe deposit, China: Controversy and ore genesis. Geosci. Front. 7, 335–344.

Fan, H.R., Yang, K.F., Hu, F.F., Wang, K.Y., Zhai, M.G., 2010. Zircon geochronology of basement rocks from the Bayan Obo area, Inner Mongolia, and tectonic implications. Acta Petrol. Sinica 26, 1342–1350 (in Chinese with English abstract).

Frost, B.R., 1991. Introduction to oxygen fugacity and its petrologic importance. In: Lindsley Donald, H. (Ed.), Oxide Minerals: Petrologic and Magnetic Significance. Rev. Mineral. Mineral. Soc. Am. 489-509.

Frost, B.R., Lindsley, D.H., 1991. Occurrence of iron-titanium oxides in igneous rocks. Rev. Mineral. Geochem. 25, 489–509.

Gaetani, G.A., Grove, T.L., 1997. Partitioning of moderately siderophile elements among olivine, silicate melt, and sulfide melt: constraints on core formation in the Earth and Mars. Geochim. Cosmochim. Acta 61, 1829–1846.

Gao, J.F., Zhou, M.F., Lightfoot, P.C., Wang, C.Y., Qi, L., Sun, M., 2013. Sulfide saturation and magma emplacement in the formation of the Permian Huangshandong Ni-Cu Sulfide Deposit, Xinjiang, Northwestern China. Econ. Geol. 108, 1833–1848.

Gaspar, J.C., Wyllie, P.J., 1983. Magnetite in the carbonatites from the Jacupiranga complex. Brazil. Am. Mineral. 68, 195–213.

Ghiorso, M.S., Sack, O., 1991. Fe-Ti oxide geothermometry: Thermodynamic formulation and the estimation of intensive variables in silicic magmas. Contrib. Mineral. Petrol. 108, 485–510.

Gourcerol, B., Kontak, D.J., Thurston, P.C., Duparc, Q., 2016. Do magnetite layers in Algoma-Type banded iron formations (BIF) preserve their primary geochemical signature? A case study of samples from three Archean BIF-hosted gold deposits. Can. Mineral. 54, 605–624.

Grigsby, J.D., 1990. Detrital magnetite as a provenance indicator. J. Sediment. Res. 60, 940–951.

Hao, Z.G., Wang, X.B., Li, Z., Xiao, G.W., Zhang, T.R., 2002. Bayan Obo carbonatite REE-Nb-Fe deposit: a rare example of Neoproterozoic lithogeny and metallogeny of a damaged volcanic edifice. Acta Geol. Sinica 76, 525–540 (in Chinese with English abstract).
Haugaard, R., Frei, R., Stendal, H., Konhauser, K., 2013. Petrology and geochemistry of the ~2.9 Ga Itilliarsuk banded iron formation and associated supracrustal rocks, West Greenland: Source characteristics and depositional environment. Precambrian Res. 229, 150–176.
Hu, H., Li, J.W., Lentz, D., Ren, Z., Zhao, X.F., Deng, X.D., Hall, D., 2014. Dissolution-reprecipitation process of magnetite from the Chengchao iron deposit: insights into ore genesis and implication for in-situ chemical analysis of magnetite. Ore Geol. Rev. 57, 393–405.
Huang, X.W., Qi, L., Meng, Y.M., 2014. Trace element geochemistry of magnetite from the Fe (-Cu) deposits in the Hami Region, Eastern Tianshan Orogenic Belt, NW China. Acta Geol Sin-Engl. 88, 176–195.
Huang, X.W., Zhou, M.F., Qiu, Y.Z., Qi, L., 2015. In-situ LA-ICP-MS trace elemental analyses of magnetite: The Bayan Obo Fe-REE-Nb deposit, North China. Ore Geol. Rev. 65, 884–899.
Huang, X.W., Sappin, A.A., Boutroy, E., Beaudoin, G., Makvandi, S., 2019a. Trace element composition of igneous and hydrothermal magnetite from porphyry deposits: relationship to deposit subtypes and magmatic affinity. Econ. Geol. 114, 917–952.
Huang, X.W., Boutroy, E., Makvandi, S., Beaudoin, G., Corriveau, L., De Toni, A.F., 2019b. Trace element composition of iron oxides from IOCG and IOA deposits: relationship to hydrothermal alteration and deposit subtypes. Miner. Deposita. 54, 525–552.
Institute of Geochemistry, Chinese Academy of Sciences (IGCAS), 1988. Geochemistry of Bayan Obo deposit. Science Press, Beijing (in Chinese).
Kamvong, T., Zaw, K., Siegele, R., 2007. PIXE/PIGE microanalysis of trace elements in hydrothermal magnetite and exploration significance: a pilot study. 15th Australian Conference on Nuclear and Complementary Techniques of Analysis and 9th Vacuum Society of Australia Congress, 21st-23rd November 2007. Melbourne, Australia: University of Melbourne.
Knipping, J.L., Bilenker, L.D., Simon, A.C., Reich, M., Barra, F., Deditius, A.P., Walle, M., Heinrich, C.A., Holtz, F., Munizaga, R., 2015. Trace elements in magnetite from massive iron oxide-apatite deposits indicate a combined formation by igneous and magmatic-hydrothermal processes. Geochim. Cosmochim. Acta 171, 15–38.
Lai, X.D., Yang, X.Y., Liu, Y.L., Yan, Z.D., 2016. Genesis of the Bayan Obo Fe-REE-Nb deposit: Evidences from Pb-Pb age and microanalysis of the H8 formation in Inner Mongolia, North China Craton. J. Asian Earth Sci. 120, 87–99.
Le Bas, M.J., Yang, X.M., Taylor, R.N., Spiro, B., Milton, J.A., Zhang, P.S., 2007. New evidence from a calcite-dolomite carbonatite dike for the magmatic origin of the massive Bayan Obo ore-bearing dolomite marble, Inner Mongolia, China. Mineral. Petrol. 90, 223–248.
Li, W., Xie, G.Q., Mao, J.W., Zhu, Q.Q., Zheng, J.H., 2019. Mineralogy, fluid inclusion, and stable isotope studies of the Chengchao Deposit, Hubei Province, Eastern China: implications for the formation of high-grade Fe Skarn deposits. Econ. Geol. 114, 325–352.
Li, X.C., Yang, K.F., Spandler, C., Fan, H.R., Zhou, M.F., Hao, J.L., Yang, Y.H., 2021. The effect of fluid-aided modification on the Sm-Nd and Th-Pb geochronology of monazite and bastnäsite: Implication for resolving complex isotopic age data in REE ore systems. Geochim. Cosmochim. Acta 300, 1–24.
Lindsley, D.H., 1991. Oxide minerals: petrologic and magnetic significance. Rev. Mineral. Mineral. Soc. Am. 25, 509.
Ling, M.X., Zhang, H., Li, H., Liu, Y.L., Liu, J., Li, L.Q., Li, C.Y., Yang, X.Y., Sun, W., 2014. The Permian-Triassic granitoids in Bayan Obo, North China Craton: A geochemical and geochronological study. Lithos 190–191, 430–439.
Liu, S., Fan, H.R., Yang, K.F., Hu, F.F., Rusk, B., Liu, X., Li, X.C., Yang, Z.F., Wang, Q.W., Wang, K.Y., 2018c. Fenitization in the giant Bayan Obo REE-Nb-Fe deposit: Implication for REE mineralization. Ore Geol. Rev. 94, 290–309.
Liu, S., Fan, H.R., Yang, K.F., Hu, F.F., Wang, K.Y., Chen, F.K., Yang, Y.H., Yang, Z.F., Wang, Q.W., 2018a. Mesoproterozoic and Paleozoic hydrothermal metasomatism in the giant Bayan Obo REE-Nb-Fe deposit: Constrains from trace elements and Sr-Nd isotope of fluorite and preliminary thermodynamic calculation. Precambrian Res. 311, 228–246.
Liu, L., Zhang, L., Dai, Y., 2014. Formation age and genesis of the banded iron formations from the Guyang Greenstone Belt, Western North China Craton. Ore Geol. Rev. 63, 388–404.
Liu, X.S., 1996. Progressive metamorphic genesis of Archean granulites in central Nei Mongol. Acta Petrol. Sinica 12, 287–298 (in Chinese with English abstract).
Liu, Y.L., Ling, M.X., Williams, I.S., Yang, X.Y., Wang, C.Y., Sun, W., 2018b. The formation of the giant Bayan Obo REE-Nb-Fe deposit, North China, Mesoproterozoic carbonatite and overprinted Paleozoic dolomitization. Ore Geol. Rev. 92, 73–83.
Liu, Y.S., Hu, Z.C., Gao, S., Gunther, D., Xu, J., Gao, C.G., Chen, H.H., 2008. In situ analysis of major and trace elements of anhydrous minerals by LA-ICP-MS without applying an internal standard. Chem. Geol. 257, 34–43.
McLennan, S.M., 1989. Rare earth elements in sedimentary rocks: influence of provenance and sedimentary processes. Rev. Mineral. Geochem. 21, 169–200.
McQueen, K.G., Cross, A.J., 1998. Magnetite as a geochemical sampling medium: Application to skarn deposits: Brisbane. Geological Society of Australia, Special Publication 20, 194–199.
Milani, L., Bolhar, R., Cawthorn, R.G., Frei, D., 2017. In situ LA-ICP-MS and EPMA trace element characterization of Fe-Ti oxides from the phoscorite-carbonatite association at Phalaborwa, South Africa. Miner. Deposita. 52, 747–768.
Mollo, S., Putirka, K., Iezzi, G., Scarlato, P., 2013. The control of cooling rate on titanomagnetite composition: implications for a geospeedometry model applicable to alkaline rocks from Mt. Etna volcano. Contrib. Mineral. Petrol. 165, 457–475.
Moon, I., Lee, I., Seo, J.H., Yang, X.Y., 2017. Geochemical studies of banded iron formations (BIFs) in the North China Craton: a review. Geosci. J. 21, 971–983.
Nadoll, P., Angerer, T., Mauk, J.L., French, D., Walshe, J., 2014. The chemistry of hydrothermal magnetite: A review. Ore Geol. Rev. 61, 1–32.
Nadoll, P., Mauk, J.L., Hayes, T.S., Koenig, A.E., Box, S.E., 2012. Geochemistry of Magnetite from Hydrothermal Ore Deposits and Host Rocks of the Mesoproterozoic Belt Supergroup, United States. Econ. Geol. 107, 1275–1292.
Nadoll, P., Mauk, J.L., Leveille, R.A., Koenig, A.E., 2015. Geochemistry of magnetite from porphyry Cu and skarn deposits in the southwestern United States. Miner. Deposita. 50, 493–515.
Nan, J.B., Huang, H., Wang, C.L., Peng, Z.D., Tong, X.X., Zhang, L.C., 2017. Geochemistry and depositional setting of Banded Iron Formations in Guyang greenstone belt. Inner Mongolia. Geol. China 44, 331–345 (in Chinese with English abstract).
Ndime, E.N., Ganno, S., Nzenti, J.P., 2019. Geochemistry and Pb-Pb geochronology of the Neoarchean Nkout West metamorphosed banded iron formation, southern Cameroon. Int. J. Earth Sci. 108, 1551–1570.
Nielsen, R.L., Beard, J.S., 2000. Magnetite-melt HFSE partitioning. Chem. Geol. 164, 21–34.
Nielsen, R.L., Forsythe, L.M., Gallahan, W.E., Fisk, M.R., 1994. Major and trace-element magnetite-melt equilibria. Chem. Geol. 117, 167–191.
Palma, G., Barra, F., Reich, M., Simon, A.C., Romero, R., 2020. A review of magnetite geochemistry of Chilean iron oxide-apatite (IOA) deposits and its implications for ore-forming processes. Ore Geol. Rev. 126.
Peng, H.J., Hou, L., Sun, C., Zou, H., Wang, T.R., Ma, Z.Z., 2021. Geochemistry of magnetite from the Hongniu-Hongshan Cu skarn deposit in Yunnan Province, SW China. Ore Geol. Rev. 136.
Ranta, E., Stockmann, G., Wagner, T., Fusswinkel, T., Sturkell, E., Tollefsen, E., Skelton, A., 2018. Fluid-rock reactions in the 1.3 Ga siderite carbonatite of the Grønnedal-Íka alkaline complex, Southwest Greenland. Contrib. Mineral. Petrol. 173, 78.
Ray, G., Webster, I., 2007. Geology and chemistry of the low Ti magnetite-bearing Heff Cu-Au skarn and its associated plutonic rocks, Heffley Lake, south-central British Columbia. Explor. Min. Geol. 16, 159–186.
Reguir, E.P., Chakhmouradian, A.R., Halden, N.M., Yang, P., 2008. Early magmatic and reaction- induced trends in magnetite from the carbonatites of Kerimasi, Tanzania. Can. Mineral. 46, 879–900.
Ribeiro Da Costa, I., Rodrigues, P.C.R., Barriga, F.J.A.S., Rona, P.A., Nunes, C.D., Vaz, P. D., 2013. Colourless aegirine in metamorphic rocks from Bayan Obo (Inner Mongolia): lack of charge transfer transitions as possible explanation. Eur. J. Mineral 25, 987–993.
Righter, K., Leeman, W.P., Hervig, R.L., 2006. Partitioning of Ni, Co and V between spinel-structured oxides and silicate melts: importance of spinel composition. Chem. Geol. 227, 1–25.
Rudnick, R.L., Gao, S., 2003. Composition of the continental crust. In: Holland, H.D., Turekian, K.K. (Eds.), Treatise on Geochemistry. Elsevier-Pergaman, Oxford, pp. 1–64.
Rusk, B., Oliver, N., Cleverley, J., Blenkinsop, T., Zhang, D.X., Williams, P., Habermann, P., 2010. Physical and chemical characteristics of the Ernest Henry iron oxide copper gold deposit, Australia; implications for IOGC genesis. In: Porter, T.M. (Ed.), Hydrothermal Iron Oxide Copper-Gold and Related Deposits: A Global Perspective. PGC Publishing, Adelaide, pp. 201–218.
Rusk, B.G., Oliver, N., Brown, A., Lilly, R., Jungmann, D., 2009. Barren magnetite breccias in the Cloncurry region, Australia; comparisons to IOCG deposits. In: Williams, P.J. (Ed.), Proceedings of the 10th Biennial SGA Meeting of the Society for Geology Applied to Mineral Deposits. The Society for Geology Applied to Mineral Deposits, Townsville Australia, 656-658.
Ryabchikov, I.D., Kogarko, L.N., 2006. Magnetite compositions and oxygen fugacities of the Khibina magmatic system. Lithos 91, 35–45.
Schilling, J., Frost, B.R., Marks, M.A.W., Wenzel, T., Markl, G., 2011. Fe–Ti oxide–silicate (QUIF-type) equilibria in feldspathoid-bearing systems. Am. Mineral. 96, 100–110.
She, H.D., Fan, H.R., Yang, K.F., Li, X.C., Yang, Z.F., Wang, Q.W., Zhang, L.F., Wang, Z.J., 2021. Complex, multi-stage mineralization processes in the giant Bayan Obo REE-Nb-Fe deposit, China. Ore Geol. Rev. 139.
Shen, B.F., 2012. Geological characters and resource prospect of the BIF type iron ore deposits in China. Acta Geol. Sinca 86, 1376–1395 (in Chinese with English abstract).
Shimazaki, H., Yang, Z., Miyawaki, R., Shigeoka, M., 2008. Scandium-bearing minerals in the Bayan Obo Nb-REE-Fe deposit, Inner Mongolia, China. Resour. Geol. 58, 80–86.
Simon, A.C., Candela, P.A., Piccoli, P.M., Mengason, M., Englander, L., 2008. The effect of crystal-melt partitioning on the budgets of Cu, Au, and Ag. Am. Mineral. 93, 1437–1448.
Singoyi, B., Danyushevsky, L., Davidson, G., Large, R., Zaw, K., 2006. Determination of trace elements in magnetites from hydrothermal deposits using the LA-ICP-MS technique. In: Abstracts of Oral and Poster Presentations from the SEG 2006 Conference, pp. 367–368.
Smith, M.P., Campbell, L.S., Kynicky, J., 2015. A review of the genesis of the world class Bayan Obo Fe–REE–Nb deposits, Inner Mongolia, China: Multistage processes and outstanding questions. Ore Geol. Rev. 64, 459–476.
Smith, M.P., Spratt, J., 2012. The chemistry of niobium mineralisation at Bayan Obo, Inner Mongolia, China constraints on the hydrothermal precipitation and alteration of Nb-minerals. Acta Geol. Sin-Engl. 86, 700–722.

Song, W.L., Xu, C., Smith, M.P., Chakhmouradian, A.R., Brenna, M., Kynický, J., Chen, W., Yang, Y.H., Deng, M., Tang, H.Y., 2018. Genesis of the world's largest rare earth element deposit, Bayan Obo, China: Protracted mineralization evolution over ~1 b.y. Geology 46, 323–326.

Sun, J., Zhu, X.K., Chen, Y.L., Fang, N., 2011. Study on Fe isotope characteristic of Bayan Obo polymetallic deposit. Acta Mineral. Sinica 32, 1016–1017 (in Chinese).

Sun, J., Zhu, X.K., Chen, Y.L., Fang, N., 2012. Fe isotope compositions of related geological formation in Bayan Obo area and their constrains on the genesis of Bayan Obo ore deposit. Acta Geol. Sinica 86, 819–828 (in Chinese with English abstract).

Sun, J., Zhu, X.K., Chen, Y.L., Fang, N., 2013. Iron isotopic constraints on the genesis of Bayan Obo ore deposit, Inner Mongolia, China. Precambrian Res. 235, 88–106.

Sun, S.S., McDonough, W.F., 1989. Chemical and isotopic systematic of oceanic basalts: implications for mantle composition and processes. Geol. Soc. London. Spec. Pub. 42, 313–345.

Tamehe, L.S., Wei, C.T., Ganno, S., Rosiere, C.A., Nzenti, J.P., Ebotehouna, C.G., Lu, G. W., 2021. Depositional age and tectonic environment of the Gouap banded iron formations from the Nyong group, SW Cameroon: Insights from isotopic, geochemical and geochronological studies of drillcore samples. Geosci. Front. 12, 549–572.

Teutsong, T., Bontognali, T.R.R., Ndjigui, P.D., Vrijmoed, J.C., Teagle, D., Cooper, M., Vance, D., 2017. Petrography and geochemistry of the Mesoarchean Bikoula banded iron formation in the Ntem complex (Congo craton), Southern Cameroon: implications for its origin. Ore Geol. Rev. 80, 267–288.

Tian, J., Zhang, Y., Gong, L., Francisco, D.G., Emil Berador, A., 2021. Genesis, geochemical evolution and metallogenic implications of magnetite: Perspective from the giant Cretaceous Atlas porphyry Cu-Au deposit (Cebu, Philippines). Ore Geol. Rev. 133.

Toplis, M., Corgne, A., 2002. An experimental study of element partitioning between magnetite, clinopyroxene and iron-bearing silicate liquids with particular emphasis on vanadium. Contrib. Mineral. Petrol. 144, 22–37.

Verdugo-Ihl, M.R., Ciobanu, C.L., Cook, N.J., Ehrig, K.J., Courtney-Davies, L., 2020. Defining early stages of IOCG systems: evidence from iron oxides in the outer shell of the Olympic Dam deposit, South Australia. Miner. Deposita. 55, 429–452.

Viehmann, S., Bau, M., Hoffmann, J.E., Münker, C., 2015. Geochemistry of the Krivoy Rog Banded Iron Formation, Ukraine, and the impact of peak episodes of increased global magmatic activity on the trace element composition of Precambrian seawater. Precambrian Res. 270, 165–180.

Wang, M., Wang, W., Liu, K., Michalak, P.P., Wei, K., Hu, M., 2017. In-situ LA-ICP-MS trace elemental analyzes of magnetite: The Tieshan skarn Fe-Cu deposit, Eastern China. Chem. Erde. 77, 169–181.

Wang, J., Tatsumoto, M., Li, X., Premo, W.R., Chao, E.C.T., 1994. A precise 232Th-208Pb chronology of fine grained monazite: age of the Bayan Obo REE-Fe-Nb ore deposit China. Geochim. Cosmochim. Acta 58, 3155–3169.

Wang, J.Y., Li, Z.D., Li, G.Y., Wen, S.B., Xie, Y., Zhang, Q., Zhang, F., Ding, N., 2019. Formation age, geochemical signatures and geological significance of the Hejiao iron deposit, Inner Mongolia. J. Earth Sci. 45, 2135–2151.

Wei, J.Y., Shangguan, Z.G., 1983. Oxygen isotope composition of magnetite and hematite in Baiyun Ebo iron deposit, Inner Mongolia. Scientia Geol. Sinica 3, 217–224 (in Chinese with English abstract).

Whalen, J.B., Chappel, B.W., 1988. Opaque mineralogy and mafic mineral chemistry of I- and S-type granites of the Lachlan fold belt, southeast Australia. Am. Mineral. 73, 281-296.

Xiao, W.J., Windley, B.F., Hao, J., Zhai, M.G., 2003. Accretion leading to collision and the Permian Solonker suture, Inner Mongolia, China: Termination of the central Asian orogenic belt. Tectonics 22. https://doi.org/10.1029/2002tc001484.

Yang, K.F., Fan, H.R., Hu, F.F., Wang, K.Y., 2012. Sediment source of Bayan Obo Marginal rift and genesis of ore-bearing dolomite of the giant REE deposit. Acta Geol. Sinica 86, 775–784 (in Chinese with English abstract).

Yang, K.F., Fan, H.R., Pirajno, F., Li, X.C., 2019. The Bayan Obo (China) giant REE accumulation conundrum elucidated by intense magmatic differentiation of carbonatite. Geology 47, 1198–1202.

Yang, K.F., Fan, H.R., Santosh, M., Hu, F.F., Wang, K.Y., 2011. Mesoproterozoic carbonatitic magmatism in the Bayan Obo deposit, Inner Mongolia, North China: Constraints for the mechanism of super accumulation of rare earth elements. Ore Geol. Rev. 40, 122–131.

Yang, X.Y., Lai, X.D., Pirajno, F., Liu, Y.L., Ling, M.X., Sun, W.D., 2017. Genesis of the Bayan Obo Fe-REE-Nb formation in Inner Mongolia, North China Craton: A perspective review. Precambrian Res. 288, 39–71.

Yang, X.Y., Lai, X.D., Ren, Y.S., Ling, M.X., Liu, Y.L., Liu, J.Y., 2015. Geological characteristics and their scientific problems of the Bayan Obo Fe-REE-Nb deposit: discussion on the origin of Bayan Obo super-large deposit. Acta Geol. Sinica 89, 2323–2350 (in Chinese with English abstract).

Zeng, M.W., Wang, M.Z., Qu, W.Z., 1981. The study on genetic mineralogy of magnetite of the Bayan Obo Fe deposit. J. Mineral. Petrol. 44–58 (in Chinese).

Zhang, L.C., Zhai, M.G., Wan, Y.S., Guo, J.H., Dai, Y.P., Wang, C.L., Liu, L., 2012. Study of the Precambrian BIF-iron deposits in the North China Craton: Progresses and questions. Acta Petrol. Sinica 28, 3431–3445 (in Chinese with English abstract).

Zhang, S.H., Zhao, Y., Liu, Y., 2017. A precise zircon Th-Pb age of carbonatite sills from the world's largest Bayan Obo deposit: Implications for timing and genesis of REE-Nb mineralization. Precambrian Res. 291, 202–219.

Zhang, Z.Q., Yuan, Z.X., Tang, S.H., Bai, G., Wang, J.H., 2003. Age and Geochemistry of the Bayan Obo Ore Deposit. Geological Publishing House, Beijing 1–205 (in Chinese with English Abstract).

Zhong, Y., Zhai, M.G., Peng, P., Santosh, M., Ma, X.D., 2015. Detrital zircon U-Pb dating and whole-rock geochemistry from the clastic rocks in the northern marginal basin of the North China Craton: Constraints on depositional age and provenance of the Bayan Obo Group. Precambrian Res. 258, 133–145.

Zhou, Z.G., Hu, M.M., Wu, C., Wang, G.S., Liu, C.F., Cai, A.R., Jiang, T., 2018. Coupled U-Pb dating and Hf isotopic analysis of detrital zircons from Bayan Obo Group in Inner Mongolia: Constraints on the evolution of the Bayan Obo rift belt. Geol. J. 53, 2649–2664.

Zhou, Z.L., Li, G.Y., Song, T.Y., Liu, Y.G., 1980. The geological features of the carbonatite in Bayan Obo and its genesis. Geol. Rev. 26, 35–42 (in Chinese).